
Electronic Thesis and Dissertation Repository

2-17-2022 2:00 PM

Visualization and manual segmentation of the post-mortem human amygdala subnuclei using ultra high field magnetic resonance imaging

Sara M. Pac, *The University of Western Ontario*

Supervisor: Khan, Ali R., *The University of Western Ontario*

: Duerden, Emma G., *The University of Western Ontario*

A thesis submitted in partial fulfillment of the requirements for the Master of Science degree in Neuroscience

© Sara M. Pac 2022

Follow this and additional works at: <https://ir.lib.uwo.ca/etd>



Part of the [Medical Neurobiology Commons](#)

Recommended Citation

Pac, Sara M., "Visualization and manual segmentation of the post-mortem human amygdala subnuclei using ultra high field magnetic resonance imaging" (2022). *Electronic Thesis and Dissertation Repository*. 8425.

<https://ir.lib.uwo.ca/etd/8425>

This Dissertation/Thesis is brought to you for free and open access by Scholarship@Western. It has been accepted for inclusion in Electronic Thesis and Dissertation Repository by an authorized administrator of Scholarship@Western. For more information, please contact wlsadmin@uwo.ca.

Abstract

The human amygdala is composed of 13 functionally and anatomically distinct subnuclei. Because most nuclei are difficult to distinguish at the microanatomical level, they are also challenging to discern macroscopically. In low field strength magnetic resonance imaging (MRI) studies, the amygdala can be identified only in its entirety. Higher resolution scans can be acquired by employing ultra-high field strength MRI acquisition techniques. We present a step-by-step guide for the manual segmentation of the amygdala subnuclei at ultra-high field 9.4T MRI. Post-mortem human brain specimen amygdala prosections fit for the 9.4T MRI bore allowed for the collection of high resolution T2-weighted images and visualization of all subnuclei. Intra and inter-rater reliability results suggest this yields a precise protocol leading to greater amygdala subnuclei labelling accuracy applicable for future research investigating substructure functions *iv vivo*. The aforementioned *ex vivo* neuroimaging methodologies can be implemented in the investigation of other subcortical brain structures.

Keywords

amygdala, amygdala subnuclei, magnetic resonance imaging, neuroimaging, post-mortem anatomy, segmentation, subcortex, ultra-high field MRI.

Summary for Lay Audience

The amygdala is a tiny almond shaped structure located deep within the brain. The amygdala's substructures are especially important due to their implications in anxiety and neurological disorders like Alzheimer's disease. Only through the use of post-mortem specimen data acquisition at ultra-high magnetic field strength MRI (magnetic resonance imaging) can we delineate the human amygdala subnuclei. MRI is a tool which uses magnetic fields and radio waves instead of x-rays to generate images of the organs within the body. When one suffers from a chronic migraine or a suspected concussion, a doctor may order an MRI scan to take a close look inside the head at the brain. MRI makes use of the water molecules throughout your body. While MRI machines are predominantly used in diagnostic medicine in patients, they can also be used to form images of post-mortem specimens. There are many types of MRI scanners, some are more powerful because the magnet is stronger. With a stronger MRI machine, resulting images may provide higher quality pictures of the brain. The more powerful the scanner, the better the result. Scanning post-mortem human brain specimens at strong MRI scanners for long periods of time without detriments like motion leads to high contrast between the grey and white matter of the brain tissue. This contrast allows for the visualization of the even smaller internal parts of the amygdala, deep within the brain.

The amygdala is imaged in its entirety at lower strength MRI but the examination of its internal details requires the improved resolution provided by ultra-high field MRI scanners. By manually contouring 13 distinct amygdala grey matter substructures individually on MRI images allowed for the development of a highly reproducible manual segmentation protocol. Segmentation of the amygdala substructures on MRI scans provided measurements of their volumes and will provide better clues of underlying *in vivo* anatomy and pathologies. If the substructures are anatomically mapped out with structural MRI, individual functions can become better understood. They may be specifically relevant to certain etiologies.

Co-Authorship Statement

Dr. Ali Khan influentially oversaw the project. He was instrumental in the decision making process during the collection of high resolution *ex vivo* ultra-high field MRI data. Without his proficient knowledge of MRI acquisition, registration and segmentation, this work would not have been possible.

Dr. Emma Duerden cultivated the motivation behind this project. She contributed significantly to the background knowledge, rationale, and teaching of skills relevant to brain neuroanatomy. Her expertise in amygdala subnuclei anatomical parcellation provided the foundation for the current work.

Daniel Cao was involved in the early stages of post-mortem specimen neuroimaging preparation and segmented several of the amygdala subnuclei from the 9.4T MRI scans in order to calculate the inter-rater reliability metrics.

Acknowledgments

Thank you to my supervisors Dr. Emma Duerden and Dr. Ali Khan for sharing your overwhelming academic knowledge. Your open-mindedness, patience, kindness, and supportive nature is unparalleled as mentors. It was truly an honour and a privilege.

We gratefully acknowledge the brain tissue donors and their families.

Thank you to the members of the CFMM at Robarts Research Institute for their guidance and helpfulness in the collection of the data. A special shout-out to Dr. Alex Li, Trevor Szekeres, and Scott Charlton for their assistance in the MRI acquisition process and protocol development.

Thank you to the members of the Khan and Developing Brain Labs for all their discussions and feedback. Thanks to Dr. Stephen Pasternak, Dr. Wataru Inoue, and Dr. Michael Jurkiewicz for providing interesting inputs at all advisory committee meetings.

Thank you to my family for their unconditional love and encouragement.

Table of Contents

| | |
|---|-----|
| Abstract..... | ii |
| Summary for Lay Audience..... | iii |
| Co-Authorship Statement..... | iv |
| Acknowledgments..... | v |
| Table of Contents..... | vi |
| List of Tables..... | ix |
| List of Figures..... | x |
| Chapter 1..... | 1 |
| 1 Introduction..... | 1 |
| 1.1 Evolutionary development of the amygdaloid complex..... | 1 |
| 1.2 Amygdala subnuclei anatomy..... | 3 |
| 1.3 Subnuclei specific amygdalar functions and connectivity..... | 6 |
| 1.4 Imaging the human amygdala..... | 9 |
| 1.5 Techniques for segmenting the human amygdala and its subnuclei..... | 12 |
| 1.6 Human amygdala subnuclei segmentation challenges..... | 14 |
| 1.7 Goal of the current study..... | 15 |
| Chapter 2..... | 17 |
| 2 Methods..... | 17 |
| 2.1 Specimens..... | 17 |
| 2.2 Specimen preparation for scanning..... | 18 |
| 2.3 MRI acquisition and pre-processing..... | 21 |
| 2.4 Manual registration of 9.4T MRI onto 7T MRI..... | 22 |
| 2.5 Target registration error (TRE)..... | 25 |
| 2.6 Manual segmentation of the 9.4T MRI amygdala..... | 26 |

| | | |
|------------|--|----|
| 2.6.1 | Paralaminar nucleus | 26 |
| 2.6.2 | Lateral nucleus | 27 |
| 2.6.3 | Basolateral nucleus | 28 |
| 2.6.4 | Basomedial nucleus | 29 |
| 2.6.5 | Corticoamygdaloid transition area (CATA) | 30 |
| 2.6.6 | Central nucleus..... | 31 |
| 2.6.7 | Medial nucleus | 32 |
| 2.6.8 | Cortical nucleus | 33 |
| 2.6.9 | Anterior amygdala area (AAA) | 34 |
| 2.7 | Ultra-high-resolution MRI and histology public datasets (BigBrain and Edlow) | 37 |
| 2.8 | Reliability measures..... | 39 |
| Chapter 3 | | 42 |
| 3 | Results | 42 |
| 3.1 | Target Registration Error | 42 |
| 3.2 | Volume measurements of amygdala subnuclei..... | 43 |
| 3.3 | Manual segmentation reliabilities of amygdala subnuclei volumes | 45 |
| Chapter 4 | | 48 |
| 4 | Discussion | 48 |
| 4.1 | Ultra-high field MRI amygdala segmentation | 48 |
| 4.2 | Amygdala subnuclei segmentation protocols | 49 |
| 4.3 | Limitations to amygdala subnuclei segmentation..... | 51 |
| 4.4 | Amygdala subnuclei manual segmentation reliabilities | 53 |
| 4.5 | Amygdala subnuclei segmentation enhancements..... | 55 |
| 4.6 | Future applications..... | 57 |
| 4.7 | Conclusion | 59 |
| References | | 60 |

Curriculum Vitae 65

List of Tables

| | |
|---|----|
| Table 1. The age and sex of the ten ex vivo human brain specimens included in this study. | 18 |
| Table 2. The averaged and range of TRE values for the x, y, and z planes of four landmark fiducials (top row) used to register 20 amygdala subnuclei scans onto their whole brain specimen counterparts..... | 42 |
| Table 3. The dice kappa intra and inter-rater coefficient reliabilities for the nine manually segmented subnuclei. Abbreviations: Lateral nucleus (La); Basolateral nucleus (BLa); Basomedial nucleus (BMe); Paralaminar nucleus (PL); Corticoamygdaloid transition area (CATA); Anterior amygdala area (AAA); Central nucleus (Ce); Medial nucleus (Me); Cortical nucleus (Co). | 46 |
| Table 4. The intraclass correlation coefficients for intra and inter-rater reliabilities as applied to the nine manually segmented subnuclei. Abbreviations: Lateral nucleus (La); Basolateral nucleus (BLa); Basomedial nucleus (BMe); Paralaminar nucleus (PL); Corticoamygdaloid transition area (CATA); Anterior amygdala area (AAA); Central nucleus (Ce); Medial nucleus (Me); Cortical nucleus (Co). | 46 |
| Table 5. The dice kappa coefficients for nine segmented amygdala subnuclei compared manually and automatically for two datasets. | 47 |

List of Figures

Figure 1. Dissection of the right human amygdala depicting the arrangement of its subnuclei: 1 lateral nucleus, 2 basolateral nucleus, 3 basomedial nucleus, 4 cortical nucleus, 5 central nucleus, 6 medial nucleus, str stria terminalis ¹³ 3

Figure 2. Neurons within the amygdala subnuclei as seen at x 200 magnification using a hematoxylin-eosin (H&E) histology stain with the neuronal cell nuclei presented in dark purple. m medial nucleus, c cortical nucleus, ce central nucleus, lat lateral nucleus, *bm* basomedial nucleus, *bl* basolateral nucleus ¹³ 5

Figure 3. A manual outline of the right amygdala of a patient suffering from narcolepsy with cataplexy (NC) and a control healthy subject as observed on a T1-weighted coronal in-vivo brain scan collected at 1.5T. 10

Figure 4. Coronal views of a T2-weighted structural Fast Spin Echo 4.7T MRI image of the amygdala and its subnuclei geometric rule groupings (d', d) delineated and classed in reference to a human brain histological atlas (i, l) ⁵¹. 13

Figure 5. The brain shaped 3D printed container holding an ex vivo human brain. 19

Figure 6. One post-mortem human brain specimen with the dura and pia mater removed from its surface. I. Lateral view II. Posterior view III. Ventral view IV. Dorsal view. 20

Figure 7. A resection of a left hemisphere MTL centered on the amygdala region (bounding box) placed in a plastic 2.5 cm cylindrical container fit for the 60 mm bore at the 9.4T MRI scanner. 21

Figure 8. 9.4T to 7T MRI registration step one. The first fiducial represented by L-0 sits at the first slice of the lateral amygdala nucleus in the bottom left hand plane. 23

Figure 9. Step two of the 9.4T to 7T MRI registration. The L-1 fiducial represents the inferior horn of the lateral ventricle at the highest level of uncus prominence. 24

Figure 10. Step three of the 9.4T to 7T MRI registration. The L-2 fiducial represents the last slice of the uncus as observed in the lower middle sagittal 9.4T brain slice. 24

Figure 11. The 9.4T amygdala scan registered with the fourth anatomical fiducial L-3 placed in the centre of the hippocampal head onto its corresponding location on the 7T scan. 25

Figure 12. Segmentation of the left PL nucleus (coronal plane) from posterior to anterior. US = Unsegmented, S = Segmented. 27

Figure 13. Segmentation of the left lateral amygdala subnucleus (coronal plane) from anterior to posterior. US = Unsegmented, S = Segmented..... 28

Figure 14. Segmentation of the left basolateral subnucleus (coronal plane) from anterior to posterior. US = Unsegmented, S = Segmented..... 29

Figure 15. Segmentation of the left basomedial subnucleus (coronal plane) from anterior to posterior. US = Unsegmented, S = Segmented..... 30

Figure 16. Segmentation of the left CATA (coronal plane) from posterior to anterior. US = Unsegmented, S = Segmented. 31

Figure 17. Left central amygdala nucleus segmentation (coronal plane) from anterior to posterior. US = Unsegmented, S = Segmented..... 32

Figure 18. The left medial nucleus parcellated starting anteriorly on the left hand side. US = Unsegmented, S = Segmented. 33

Figure 19. The amygdala’s left cortical nucleus (coronal view) segmented from the anterior to posterior. US = Unsegmented, S = Segmented..... 34

Figure 20. The AAA parcellated at the left amygdala’s anterior end. US = Unsegmented, S = Segmented..... 35

Figure 21. The 9.4T high resolution scans (bottom right) outlined in reference to the 7T whole brain ex vivo specimens (left) from which they were derived. The legend (top right) includes the coloured-labelling for seven out of nine visible amygdala subnuclei. 36

Figure 22. The amygdala subnuclei segmented from the anterior end at the top left to the posterior end at the bottom right. The first and third rows represent the registered MRI images through some representative amygdala slices while the second and fourth rows

represent their respective parcellated amygdala subnuclei slices. The amygdala subnuclei legend here is continued from Figure 21. 37

Figure 23. A slice through the left human amygdala unsegmented, manually segmented, and automatically segmented from ultra-high resolution MRI and histology data. 39

Figure 24. 3D rendering of the left amygdala and its substructures from anterior and inferior viewpoints. The legend for subnuclei can be found in Figures 21 and 22..... 44

Figure 25. The raw and relative amygdala subnuclei volumes. Abbreviations: Lateral nucleus (La); Basolateral nucleus (BLa); Basomedial nucleus (BMe); Paralaminar nucleus (PL); Corticoamygdaloid transition area (CATA); Anterior amygdala area (AAA); Central nucleus (Ce); Medial nucleus (Me); Cortical nucleus (Co). 45

Figure 26. A clinical human amygdala specimen with three processed histological slices on the right hand side co-registered with the 9.4T MRI scans presented on the left. 57

Chapter 1

1 Introduction

For an admittedly small quantity of brain tissue, the amygdala has a great degree of importance in the central nervous system. As a member of the limbic system, it functions to control autonomic nervous system responses including changes in blood pressure and heart rate, which accompany the structure's well known involvement in emotional manifestations, namely fear and anxiety¹. It also processes auditory and olfactory stimuli, and has even become a marker of epileptogenic foci in cases of temporal epilepsy^{2,3}. In large part, the functional identity of the amygdala is clear.

It is the anatomical characteristics of the amygdalae which demand a more thorough investigation. The amygdala is a brain structure perched atop the hippocampus located bilaterally in the anteromedial part of the brain's temporal lobes. Designated as the amygdaloid nuclear complex, the amygdala is made up of non-homogenous islets of grey matter. Each amygdalar nucleus is functionally and anatomically distinct. This thesis will depict the neuroanatomy of the amygdala's multiplicity of nuclei with accuracy through the use of ultra-high field (UHF) magnetic resonance imaging (MRI) and post-mortem specimen data collection. Localizing the nuclei of the amygdala is a challenging task but made possible with high resolution neuroimaging acquisition techniques. A labelling protocol of the discrete amygdala subnuclei will be outlined. With a complete structural mapping of the amygdala subnuclei, functional organization at the substructure level will become better understood when overlaid in combination in future *in vivo* applications.

1.1 Evolutionary development of the amygdaloid complex

As a consequence of Urbach-Wiethe disease, patient S.M. suffered complete and exclusive destruction to her bilateral amygdalae¹⁶. She revealed no fear responses while watching horror film clips, walking through a haunted sanatorium attraction or in the presence of tarantulas and snakes. Patient S.M. has been described as behaving without inhibition in social situations and exhibiting high positive affect despite the adversities in her life¹⁷. Her case has helped elucidate the fear basis of the structure's role.

Fear is central to the evolution of the mammalian brain and the amygdala is an evolutionarily conserved structure⁷. From amphibian, reptile, and mammal data, it seems the amygdalae evolved not as the sum of unrelated substructures but occurring through a common stream of migrating cells derived from the telencephalon neocortex⁸. For example, accessory olfactory bulb (AOB) neurons arising in the telencephalon target the amygdaloid complex. This migratory stream is conserved in the African-clawed frog (*Xenopus*)⁹. In tailless amphibians like frogs, the AOB projects to the lateral amygdala nucleus^{10,11}. In reptiles the AOB extends to the anterior amygdala area, and in mammals to the cortical and medial nuclei¹².

Based on these olfactory projections, certain amygdalar nuclei appear to have comparable topological positions that may be homologous across species. These homologous regions allow for complex forms of emotional learning such as fear conditioning¹⁸. The amygdala responds to sensory input like smell from the vomeronasal organ in the nose of animals extending to the AOB that allows for associative learning between odors and behavioural responses. Rats exposed to cat odors learned to spend a majority of time hidden in a box suggesting fear conditioning occurred via the olfactory pathway to the medial amygdala¹⁹.

Yet not all anatomical subdivisions of the amygdala may be easily distinguishable especially among amphibian and reptile species. In mammals there is clearer evidence that two divisions of the telencephalon, the pallium and subpallium, drive migratory and morphogenetic processes during the development of the amygdala. The pallial component of the telencephalon first forms the roof of the cerebral ventricles while the subpallium forms the thickening of the floor of the ventricles¹³. During mammalian embryonic development, some researchers postulate that the pallium participates in the formation of the lateral, basolateral and basomedial amygdala nuclei while the central, medial and cortical nuclei have the subpallium as their origin¹⁴.

Based on one long-standing idea, the organization of the amygdaloid complex consists of grouping the cortical, medial and central nuclei descended from the subpallium as the phylogenetically older group and the basomedial, basolateral, and lateral nuclei derived from the pallium as phylogenetically more recent¹⁵. The phylogenetically primitive or

old group is associated with the olfactory system while the phylogenetically new group with the neocortex. Over the years anatomists have outlined numerous methods of grouping the amygdala's substructures.

1.2 Amygdala subnuclei anatomy

The amygdala is a Greek derived word denoting an almond-shaped cluster of nuclei as discovered by Burdach in the early 19th century ⁴. Meynert provided a detailed anatomical description of the overall structure within each brain hemisphere in 1867 ⁵. In 1923, Johnston introduced a method of further subdividing the amygdala's nuclei. It was Johnston who proposed subdividing the amygdala into a primitive group of nuclei and a phylogenetically newer group ⁶. Much debate has since ensued, and continues to this day, regarding the anatomical partitioning methodology of the amygdala.

The amygdala is not a single mass. It is composed of distinct subareas. Researchers generally agree in affirming the amygdala as a heterogenous assembly of grey matter cellular islands referred to as subnuclei. Anatomists disagree on the exact number of nuclei. Crosby and Humphrey, like Johnson, parcellated the amygdala into two groups: the phylogenetically older more superficial central, cortical and medial nuclei, and the phylogenetically more recent deep lateral, basolateral, and basomedial nuclei ¹⁵. These 6 subnuclei are physically distinct on a careful gross anatomical dissection of the human amygdala (Figure 1).

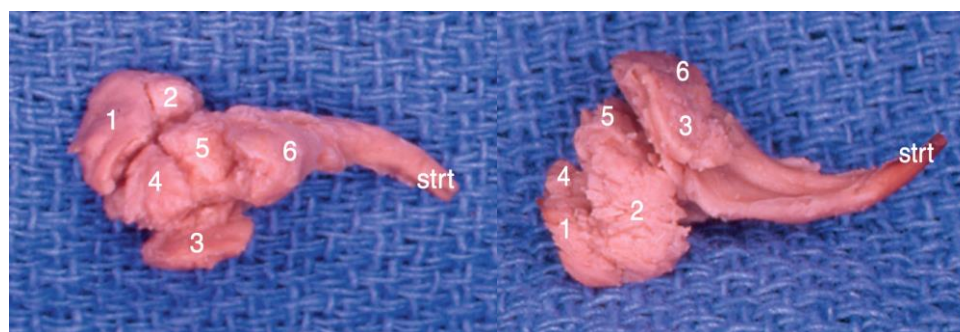


Figure 1. Dissection of the right human amygdala depicting the arrangement of its subnuclei: 1 lateral nucleus, 2 basolateral nucleus, 3 basomedial nucleus, 4 cortical nucleus, 5 central nucleus, 6 medial nucleus, str stria terminalis ¹³.

The lateral, basolateral, basomedial, cortical, central, and medial amygdala subnuclei are consistently registered nuclei across human research studies. The literature contains variations in nomenclature. The basolateral nucleus is sometimes named the basal nucleus while the basomedial nucleus may be called the accessory-basal nucleus. Throughout this work, the lateral, basolateral, and basomedial nuclei classification will be employed. Together, these three subnuclei are often referred to as the basolateral complex or basolateral amygdala (BLA), not to be confused with the basolateral nucleus of the amygdala.

Upwards of 30 amygdala nuclei have been indexed ²⁰. In these occurrences, anatomists decided to further subdivide each nucleus into multiple spatial partitions. For instance, the cortical nucleus splits into the anterior cortical and posterior cortical nuclei. Or, in a more comprehensive case, the lateral nucleus bisected into a lateral portion and a medial portion, each additionally consisting of a dorsal and ventral division ²¹. The premise behind these partitions is the underlying microanatomy or histology of amygdalar tissue.

Neurons, specialized cells which transmit nerve impulses in the brain, help partially differentiate amygdalar subnuclei locations. De Olmos's exhaustive protocol of subdividing 30 subnuclei is explained by the fact that certain types of neurons are present in particular subareas of the structure ²¹. Medium-sized spiny neurons characterize the lateral portion of both the central and medial subnuclei. The basolateral amygdala nucleus contains either nonpyramidal small neurons without spiny dendritic extensions or pyramidal neurons with spiny dendrites. While these parcellations were attempted, they are quite arbitrary as more than one type of neuron may cohabit a single nucleus or be present in multiple. Histological microscopic data depicts a rather homogenous assembly of medium-sized neurons throughout all amygdala subnuclei (Figure 2). Only minor variations occur like the medial nucleus containing smaller neurons ¹³.

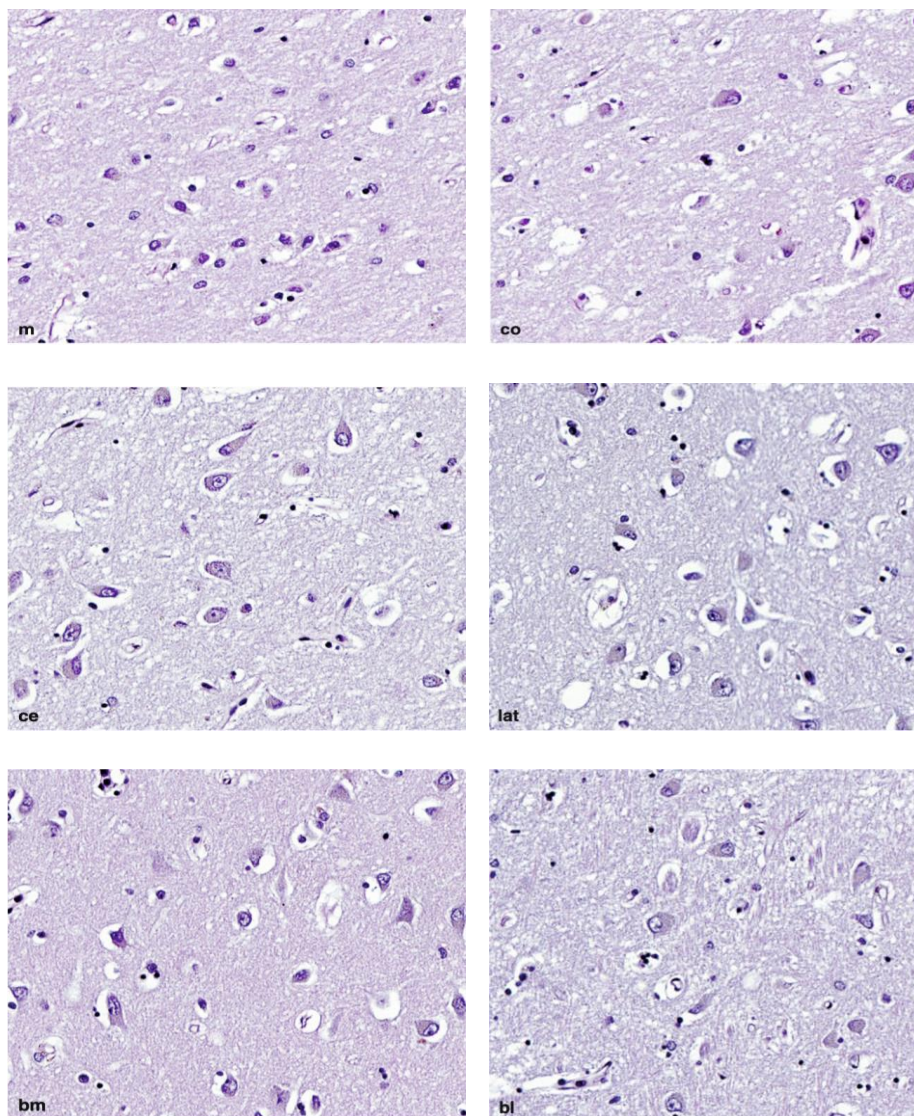


Figure 2. Neurons within the amygdala subnuclei as seen at x 200 magnification using a hematoxylin-eosin (H&E) histology stain with the neuronal cell nuclei presented in dark purple. m medial nucleus, c cortical nucleus, ce central nucleus, lat lateral nucleus, bm basomedial nucleus, bl basolateral nucleus ¹³.

Evidently, it is difficult to differentiate amygdalar subnuclei and their potential spatial divisions at a microscopic level. A more macroscopic viewing provides a clearer picture as the amygdaloid nuclei are sometimes separated and surrounded amongst one another by envelopes formed from axonal neuronal projections ¹³. Generally, the amygdala comprises approximately 13 subnuclei structural divisions ²². These include the BLA,

central, cortical, and medial nuclei as well as the paralaminar nucleus, anterior amygdaloid area, corticoamygdaloid transition area, intercalated cell nuclei, and the extended amygdala includes the amygdalo-hippocampal area, the substantia innominata, and the bed nucleus of the stria terminalis (BNST) ²³.

The paralaminar nucleus (PL) is an obscure and relatively unknown amygdala nucleus. It lies in a line inferior to the BLA. Even without a clear fiber acting as a separation, it can be distinguished by its neuronal cells which appear more densely stained because they are smaller in size and closely packed ²⁴. The PL has been an elusive subarea to study because a consensus over its nomenclature has not been reached. Other researchers have identified it as the medial part of the basolateral nucleus or named it the granularis. The anterior amygdaloid area (AAA) and the intercalated cell (IC) nuclei are also not easily grouped. The IC nuclei are located between the central and basolateral nuclei. Although the AAA lacks the nucleus designation in its name, it is still considered one of the amygdala's nuclei. It rests at the anterior end of the amygdala bordering the corticoamygdaloid-transition area (CATA) laterally. The CATA lies at the medial border of the amygdala surrounding the uncus, the parahippocampal gyrus's anterior extremity. While the extended amygdala nuclei will not be the focus of this work, they increase the functional capacity of the amygdala structure from which they are derived.

1.3 Subnuclei specific amygdalar functions and connectivity

The extended amygdala macrostructure is often overshadowed by the amygdala itself ²⁵. It is thought to be involved in the evaluation of a sensory stimuli's emotional value, and becomes activated following changes from neutral to emotional facial expressions ²⁶. The extended amygdala macrostructure is also implicated in reward cognition and through its subcortical information it relays reciprocally among the cortex, thalamus, and brainstem areas ²⁷. Some researchers regard the central and medial amygdala nuclei as a part of the extended amygdala due to histological and cytoarchitecture similarities. Nevertheless, it extends to the medial and central nuclei in particular.

The central nucleus located on the outskirts of the amygdala forms a continuum with the BNST of the extended amygdala. As the major output nucleus of the amygdala, it is in a strategic position to mediate aspects of anxiety and fear by projecting neurons to hypothalamus, brainstem, and basal forebrain, brain structures themselves involved in mediating stress responses²⁹. Fear memories are thought to be stored within these neuronal connections. From animal studies, researchers have found that the central nucleus is vital to the genesis of freezing, neuroendocrine stress hormone release, and autonomic nervous system (changes in heart rate and blood pressure) types of fear responses. It acts as an eminent somatic and visceral effector since it directly targets the spinal cord and brainstem¹³. The central nucleus is sometimes termed the nociceptive amygdala because hyperactivity in this nuclear area accounts for anxiety-like and pain-related emotional responses³⁰. Highly processed information from the BLA is transferred to the central nucleus with neurons projecting to modulatory pain systems in the brainstem and basal forebrain. Because the central nucleus is an output nucleus, it is also therefore the main recipient of inputs from the deep and superficial amygdala nuclei²⁸.

The lateral nucleus of the BLA is considered the major input nucleus of the amygdala. Sensory systems including the auditory, somatosensory (such as pain), taste, visual, and olfactory systems send information to this nucleus for dissemination³¹. In contrast, the medial nucleus receives input only from the olfactory cortex via the olfactory bulb and as such is implicated in pheromone processing and the sense of smell³⁵. The most thoroughly studied systems have been auditory connections from the auditory cortex and auditory thalamus as connected to the lateral amygdala nucleus. This notion has been used to investigate fear conditioning in animals using the acoustic startle reflex. A conditioned stimulus such as a loud high pitched startle sound is often paired with a painful foot shock and animals are trained to associate this pairing as unpleasant under certain circumstances. Following training, lesions to the auditory thalamus completely blocked the fear-potentiated startle to the auditory conditioned stimulus suggesting the lateral nucleus is involved in the integration of sensory information like audition and the neural circuit mediating classical fear conditioning³².

Light and electron microscope techniques have shown that neuronal fibers from the lateral nucleus project to the neighbouring basolateral nucleus of the amygdala³³. The lateral nucleus sends projections to the central nucleus directly but also indirectly by passing through the basolateral amygdala nucleus. Both nuclei neuronal projections may also diverge to the IC nuclei prior to reaching the central nucleus³¹. The IC nuclei are considered an ‘off switch’ as they inhibit the amygdala’s basolateral nucleus neurons and central nucleus output neurons. These intercalated clusters contain GABAergic inhibitory neurons and are thought to be involved in emotional processing because the activation of such neurons is stronger (as represented by neuronal impulse activity) after fear extinction³⁶. In fear extinction training, a conditioned stimulus first presented produces fear recall that ensures the activation of the IC nuclei but persistent presentation of the conditioned stimulus is what leads to inactivation of the IC nuclei³⁷.

Similar to the lateral nucleus, widespread reciprocal projections have been found between the basolateral nucleus and the midbrain’s inferior colliculus, the integration center of the ascending auditory system³⁴. The feedback circuit of the thalamoamygdalocollicular ascending sensory pathway involves processing the emotional content of sensory stimuli. The basolateral nucleus also sends projections to the striatum controlling actions such as running away from danger and to safety³¹. This is in contrast to the central amygdala’s connection with the brainstem whereby the control of emotional reactions like freezing in the place of a predator occurs. There are no conscious cognitive involvements to such responses within the BLA and central nucleus functionality in terms of sensory inputs, integration, and behaviour. A fight-or-flight response in reaction to a perceived harmful event is reflexive with conscious processing typically occurring after the event³⁸.

The corticoamygdaloid transition area is a zone of confluence for the basomedial nucleus BLA and paralaminar nucleus, and provides the main yet more restricted input to the central nucleus in comparison to the BLA nuclei⁴⁰. As a member of the BLA, the basomedial nucleus has neuronal fiber innervations to fellow amygdala central, medial, and AAA nuclei regions but also to the hippocampal CA1 subregion, additionally facilitating the encoding of associative fear memories³⁹.

The paralaminar nucleus also receives afferent inputs from the hippocampus and lateral amygdala nucleus to lend a supportive role in contextual learning. This nucleus contains dense innervation of serotonergic fibers as well as high concentrations of benzodiazepine, and corticotropic releasing hormone receptors ²⁴. In fact, most amygdala subnuclei are modulated by the serotonin neurotransmitter. Serotonin levels increase within the amygdala during fear memory acquisition and expression. While each amygdala subnucleus is functionally distinct, together their connections are key players in the processing of fear.

1.4 Imaging the human amygdala

The amygdaloid complex has been the focus of much functional magnetic resonance imaging (fMRI) research. In fMRI studies, participants undergo a task in an MRI scanner, and researchers obtain a better understanding of the function of a structure based on blood oxygen level dependent (BOLD) imaging responses. In one study, patients with Post-Traumatic Stress Disorder exhibited an exaggerated fMRI BOLD intensity change within the amygdala region when observing fearful versus happy facial stimuli displayed within a 1.5 Tesla (T) scanner ⁴¹.

Structural neuroimaging studies have also investigated the role of the amygdala in various neurological and psychiatric disorders. Often, structural magnetic resonance imaging (sMRI) investigations report the volumetric size of a particular brain structure when comparing clinical and control groups. A meta-analysis found that the bilateral amygdala volume was reduced in pediatric bipolar disorder ⁴². Narcolepsy patients were observed to have a 17% reduction in bilateral amygdalar grey matter volume compared to healthy volunteer participants (Figure 3) ⁴³. In depressed individuals on medication, amygdala volume was significantly increased while in unmedicated individuals with major depressive disorder, amygdala volume was significantly decreased relative to healthy persons ⁴⁴. In a meta-analysis of 23 studies, autism spectrum disorder patients had significantly larger right amygdala volumes compared to controls but no significant difference was found in left amygdala volumes ⁴⁵. These studies are conducted *in-vivo* and often using low magnetic field strength (1.5T, 3.0T) MRI scanners available at hospital and research institutions.

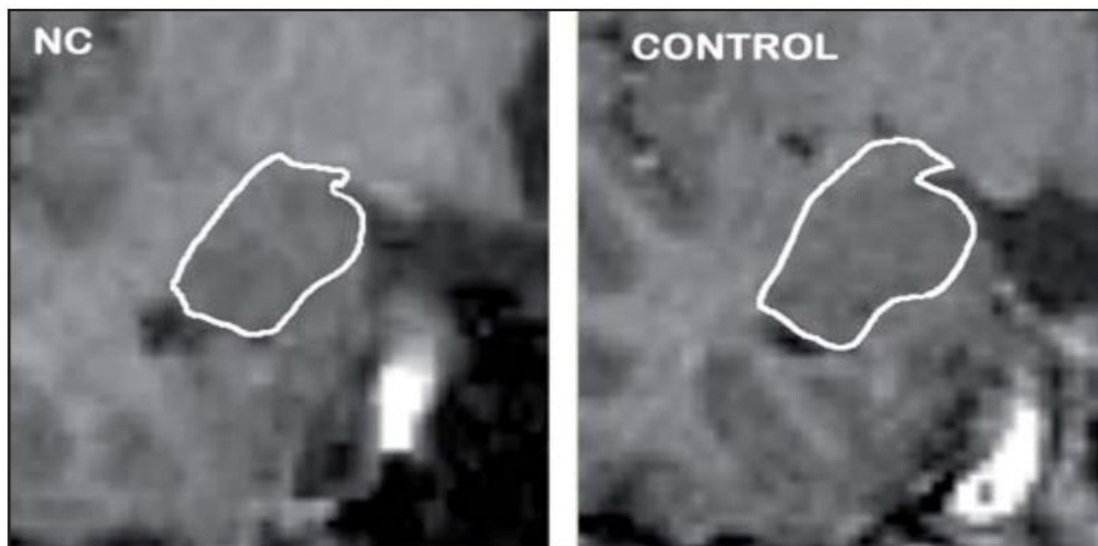


Figure 3. A manual outline of the right amygdala of a patient suffering from narcolepsy with cataplexy (NC) and a control healthy subject as observed on a T1-weighted coronal in-vivo brain scan collected at 1.5T.

As a whole entity, the amygdala is easily imaged functionally and structurally. However, obtaining the anatomical detail necessary to delineate the 13 amygdala subnuclei is challenging and requires advanced neuroimaging techniques. T1-weighted and T2-weighted scans are the most common MRI sequences. T1-weighted images are produced by using a short repetition time (TR) and a short time to echo (TE) and are characterized by grey matter appearing darker than white matter brain tissue. T2-weighted images yield scans where grey matter appears lighter than white matter as a result of longer TR and TE times. TR and TE are pulse sequence timing parameters underlying the MRI acquisition process itself based on the magnetization properties of atomic nuclei. TR is the amount of time between successive MRI pulse sequences applied to a single brain slice while TE is the time between the Radio Frequency (RF) pulse delivery and the top of the echo signal or spin echo receipt. Often, there may be more than one RF pulse in a pulse sequence, but normally there is only one excitation RF pulse per TR.

Coronal T1-weighted three-dimensional images are traditionally the more common method of measuring the volume of the amygdala as a whole. More recently, T2-weighted MRI images have been used to delineate the amygdala structure as an entity

even in neonate brain scans where drawing the amygdala to its outline is comparatively more challenging than in adult images⁴⁶. T2-weighted MRI acquisition is often the chosen method of segmenting the nearby hippocampus structure in its entirety. This contrast type also gives rise to the ability to parcellate the different hippocampal subregions⁴⁷. In neuroimaging, T2-weighted images are utilized because they are more sensitive to a wide range of pathology including information about the proton density or amount of water in each pixel, the smallest sampled two dimensional element of an MRI image⁴⁸. An MRI voxel is the volume element of a pixel defined in three dimensional space. While the amygdala subnuclei are islets of grey matter not easily separated by white matter tracts as proxied by proton density, the slight pockets of separation formed between nuclei from axonal connectivity projection innervations may aid in delineating amygdalar subnuclei when employing T2-weighted imaging protocols. High resolution T2-weighted images have been shown to deliver more suitable contrast properties for the nearby hippocampal subfield delineation even with its more complex structure and its composition of different cell compartments, offering promise for the amygdala region⁴⁷.

A major factor in determining the quality of MRI acquisition techniques is the magnetic field strength of the MRI scanner. Over the last several decades, MRI scanners in hospital and university research institutions have been those of lower magnetic field strength (i.e., 1.5T, 3.0T). At lower magnetic field strengths, outlining even the amygdala structure as a whole may be difficult because of the relatively featureless grey matter (GM) and white matter (WM) distinction. With recent advances in technology, higher field strength scanners (e.g. 7.0T, 9.4T, 11.7T) designated as ultra-high field MRI scanners allow for the acquisition of higher signal-to-contrast ratios important for yielding higher resolution scans thus clearer separation between GM and WM. With sMRI and fMRI *in-vivo* studies at low magnetic field strength and at 7T, participants lie in the scanner for a limited amount of time due to comfort and scans are prone to artifacts because of movement. Scans obtained in these cases are usually of the entire brain rather than an isolated slab of a particular structure. The highest field strength scanners like the 9.4T and 11.7T have a much smaller bore or opening such that human participant scanning *in-vivo* is rendered essentially impossible. In these instances, *ex vivo* human brain specimens may be imaged instead with a focus on acquiring brain slices only in a small brain structure like the

amygdala. As such, the *ex vivo* amygdala can be imaged for longer scanning periods, and higher resolution scans may be obtained as a result of smaller voxel sizes with powerful bores. A higher in-plane resolution such as $0.1 \times 0.1 \text{ mm}^2$ may be possible when using an ultra-high field scanner that would not have been possible when scanning the whole brain with a typical $1.0 \times 1.0 \text{ mm}^2$ in-plane resolution at lower magnetic field strength in a shorter time frame. Thinner slice thickness may also be permitted at higher field strength scanners resulting in greater anatomical detail to aid in the viewing of the amygdala subnuclei. These scans can be averaged and upsampled in post-processing steps to create even higher signal-to-contrast ratio images for segmentation purposes.

1.5 Techniques for segmenting the human amygdala and its subnuclei

With sMRI, a key step of neuroimaging processing is obtaining surface-based also known as voxel-based segmentation. Voxel-based segmentation results in the volumetric measurement of an anatomical structure within an MRI image. Volume rendered images collected from sMRI scans can be partitioned into multiple segments representing brain structures like the human amygdala and its subnuclei. There are multiple techniques for the segmentation or the outlining of the amygdala and amygdalar substructures to obtain morphology or volumes.

The basis of the MRI segmentation process for all brain structures including the amygdala involves deciding on anatomical landmarks in reference to the entire structure and its components. One study aimed to minimize the discrepancies between the segmentation protocols of different researchers striving for a consensus amygdala and hippocampus segmentation protocol and their high-resolution MRI volumetry outputs ⁴⁹. Some anatomical landmarks used to delineate the amygdala structure included the alveus or inferior horn of the lateral ventricle at the posterior end and the superior border arbitrarily defined by the drawing of a horizontal line between the optic tract's superolateral part and the inferior portion of the insula's circular sulcus. In another *in vivo* 4.7T MRI study, the amygdala was labelled using indirect geometric rules, approximating rather than more accurately parcellating each individual amygdala subnucleus ⁵⁰. They did not obtain high enough resolution at lower field strength 4.7T

MRI to depict the amygdalar subnuclei instead relying on an *ex vivo* based cytoarchitecture anatomical atlas and grouped amygdala nuclei together (Figure 4)⁵¹.

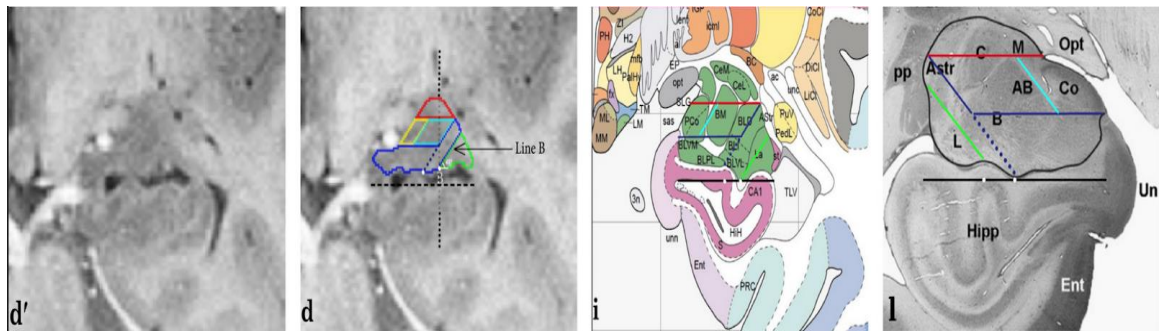


Figure 4. Coronal views of a T2-weighted structural Fast Spin Echo 4.7T MRI image of the amygdala and its subnuclei geometric rule groupings (d', d) delineated and classed in reference to a human brain histological atlas (i, l)⁵¹.

Manual segmentation is still considered the gold standard when it comes to conducting volumetric brain structure research⁵². There are very few studies which delineate the human amygdala subnuclei and report their volumetry in contrast to the copious hippocampus segmentation protocols⁴⁷. Anatomical landmarks used to parcellate the amygdala and its subnuclei are typically identified on *ex vivo* histological staining where a close look at the microscopic cytoarchitectural difference is needed to decipher amongst substructures. Mai and colleagues published an atlas of the human brain presenting the brain's anatomy at macroscopic and microscopic levels⁵¹. One aid to parcellation is referencing an already existing and labelled anatomical atlas at the microscopic level while mapping out the subregions at a more macroscopic level such as with sMRI images. Another popular human brain atlas used to reference the amygdala subnuclei histology is Duvernoy's seminal monograph mostly concentrated on the hippocampus⁵⁴. Architectonic probabilistic maps were first developed for the superficial (cortical and anterior amygdala area), centromedial, and BLA nuclei using *ex vivo* histological data derived from ten individuals⁵³.

By aligning structures visible in example histological *ex vivo* samples to the same structural boundaries in an MRI image, researchers can predict subnuclei borders and describe their anatomical location and morphologies with greater precision. This is a

labour intensive and sometimes subjective process requiring anatomical expertise. Typically on a sMRI scan, coronal, horizontal, and axial views are all observed in combination throughout a segmentation protocol. On a slice-by-slice basis, each view may illustrate a particular subnucleus with a more evident appearance. For example, the smallest cortical nucleus is usually most discernible in coronal MRI slices. With a consistent labelling protocol, a relatively straightforward list of instructions for segmenting each amygdala subnucleus can be created to describe substructure borders with a reasonable degree of reliability and accuracy. This work represents an unified attempt to determine current amygdala subnuclei segmentation challenges and to pool already existing parcellation protocols into agreement.

1.6 Human amygdala subnuclei segmentation challenges

Compared to the hippocampus, the amygdala is a more problematic structure to segment because there is little contrast variation within its make-up that could obviously separate any intra-white matter borders between subnuclei due to the low content of the myelin WM sheath⁵³. The individual BLA nuclei at their superior end are innervated by axonal connectivity projections towards the central nucleus and extended amygdala. However, WM boundaries between these largest subnuclei become increasingly more difficult to observe moving more inferiorly throughout coronal slices. The border between the CATA and basomedial nucleus is also challenging to make out. The cortical nucleus being the smallest is the hardest to parcellate as it is wedged between the CATA and basomedial nucleus and usually appears in the fewest number of MRI brain scan slices. Because they are considered a bundle of molecular cells, the IC nuclei cannot readily be picked up with the human eye at the more macroscopic MRI level even at ultra-high resolution. The paralaminar nucleus is more easily distinguished by its densely stained small closely packed neuronal banded appearance underneath the BLA. Yet many studies do not include the paralaminar nucleus in their segmentation protocol or instead consider it part of the inferior portion of the basolateral amygdala nucleus only. There is a lack of consensus of substructure nomenclature and number of nuclei compartmentalization. A major gap in the literature is the lack of a standardized method regarding gross

anatomical landmarks or subnuclei specific cues in MRI protocols segmenting the amygdala subnuclei or in its registration processes. As is true of almost all brain anatomy, individual subnuclei differences between specimens, subjects or hemispheres may exist. However, there are generally no discernable patterns of irregularities in the morphology or location of amygdalar substructures.

MRI imaging constraints are the main cause of discrepancies amongst amygdala segmentation protocols. The majority of research has taken place at lower field strength MRI scanners where the *in-vivo* amygdala is only distinguishable as the sum of its parts. Only more recently has there been leeway to employ higher field strength MRI scanners to determine *ex vivo* substructure boundaries. One paper conducted at 7T MRI used the T1-weighted acquisition to image ten *ex vivo* specimens at ultra-high field resolution yielding 9 total amygdala subnuclei segmentations from which an automated atlas was developed⁵⁵. This automated atlas propagating 9 amygdala subnuclei as manually segmented by an expert was released as part of a pipeline offered in the Freesurfer 7.1 software package. This segmentation and pipeline can be applied well to other datasets. Yet it is not entirely reliable due to inconsistencies in the registration process. The automated segmentation output often takes over the inferior horn of the lateral ventricle or supersedes its overlay onto the hippocampal head or the uncus thus shifting the correct placement of each individual amygdalar substructure⁵⁶. While automated atlases have notable strengths especially in saving time lost to manually segmenting hundreds of MRI scans, any error such as that of registration will become systematic and carried forward to all automatically segmented amygdala subnuclei.

1.7 Goal of the current study

In the present study we aim to develop a comprehensive protocol for the segmentation of amygdala subnuclei. We will overcome previous challenges of published amygdalar protocols by taking advantage of structural MRI technical advances including: ultra-high field strength 9.4T image acquisition, *ex vivo* human brain specimens allowing for increased averaging scan time, high in-plane and thin slice thickness voxel methods to improve the visibility of subnuclei. The manual segmentation of a post-mortem dataset will give rise to a robust and complete reference for future subcortical structural MRI

investigations whether in the amygdala in particular or acquisition techniques to be used in similarly difficult to delineate structures. We will be the first to outline a reliable registration technique that will be used as guidance in the segmentation protocol. Target registration errors and intra and inter rater reliabilities will determine the accuracy and reliability of these proposed gold standard amygdala subnuclei manual segmentation study goals.

Chapter 2

2 Methods

This section outlines the particulars of the post-mortem specimens, their scanning preparation, the *ex vivo* neuroimaging protocol, and the amygdala subnuclei anatomical segmentation instructions.

2.1 Specimens

Ethics was approved in accordance with Western University's Human Research Ethics Board. Post-mortem human brain specimens were procured through the Department of Anatomy and Cell Biology's Body Bequeathal Program. Bodily specimens were donated to the Body Bequeathal Program from University Hospital in London, Ontario, Canada. Ten human brain specimens were obtained in total. The participants from which the specimens were obtained did not pass away due to any neurological disorders or diseases. The average age at the time of death was 71.7 and three (30%) of the specimens were from female participants. Age and sex information for each participants' post-mortem specimen are detailed in Table 1.

Table 1. The age and sex of the ten *ex vivo* human brain specimens included in this study.

| Specimen | Sex | Age at time of death |
|-----------------|------------|-----------------------------|
| 2054 | F | 59 |
| 2070 | M | 84 |
| 2073 | M | 75 |
| 2079 | M | 88 |
| 2081 | M | 81 |
| 2082 | M | 68 |
| 2087 | F | 76 |
| 2091 | M | 81 |
| 2092 | M | 50 |
| 2094 | F | 55 |

2.2 Specimen preparation for scanning

Whole human brain specimens acquired from the Department of Anatomy and Cell Biology were stored in 10% formalin then transferred to a 1% phosphate-buffered saline (PBS) solution. Specimens were kept in a refrigerator at Robarts Research Institute in London, Ontario, Canada throughout the duration of the study.

An in-house air-tight polycarbonate 3D printed brain mold (53 cm length x 43 cm width) was developed to hold the *ex vivo* whole brain specimens (Figure 5). The brain shaped holder (cerebellum + cerebral hemispheres) was equipped with a silicone ring between its centre and two degassing ports at each end. A syringe and a tube were latched onto the

degassing port at one end and a solution named fomblin was injected into the brain holder containing the specimen. The other degassing port was kept open until the container was filled to reduce any air bubbles formed within. Fomblin (Solvay Specialty Polymers) is a colourless solution that lacks any magnetic resonance (MR) signal. It has a magnetic susceptibility similar to that of tissue resulting in MR-images with a higher contrast-to-noise ratio (CNR). One specimen at a time was placed into the container then filled with the fomblin solution for a minimum of 12 hours at room temperature in preparation for MRI scanning. All preparation steps were carried out underneath a fume hood.



Figure 5. The brain shaped 3D printed container holding an ex vivo human brain.

Prior to the scanning of the intact post-mortem human brain specimens at 7T MRI, the spinal cord, dura mater, and pia mater were separated from the tissue surface (Figure 6). The dura and pia mater were removed to ensure the fomblin became better immersed within the brain's gyri and ventricles leading to a reduction in air bubbles and increased magnetic susceptibility. Blood vessels were cut with scissors for the similar reasons not

to cause image artefacts. After each whole brain specimen scan, the fomblin was siphoned from the container to be reused for the next specimen.

The brain specimens were first dissected along the longitudinal axis into two cerebral hemispheres. Cuts were next made along the Sylvian fissure to dissect for the medial temporal lobes (MTL). A scalpel was used to cut the MTL portion to the parahippocampal sulcus landmark, the marker for the outer border of the hippocampus and the amygdala while leaving the uncus untouched on the medial side (Figure 7). A plastic cylindrical test tube container with a 2.5 cm diameter padded with gauze around the amygdala tissue and filled with fomblin was prepared for the 9.4T MRI scanning (Figure 7).

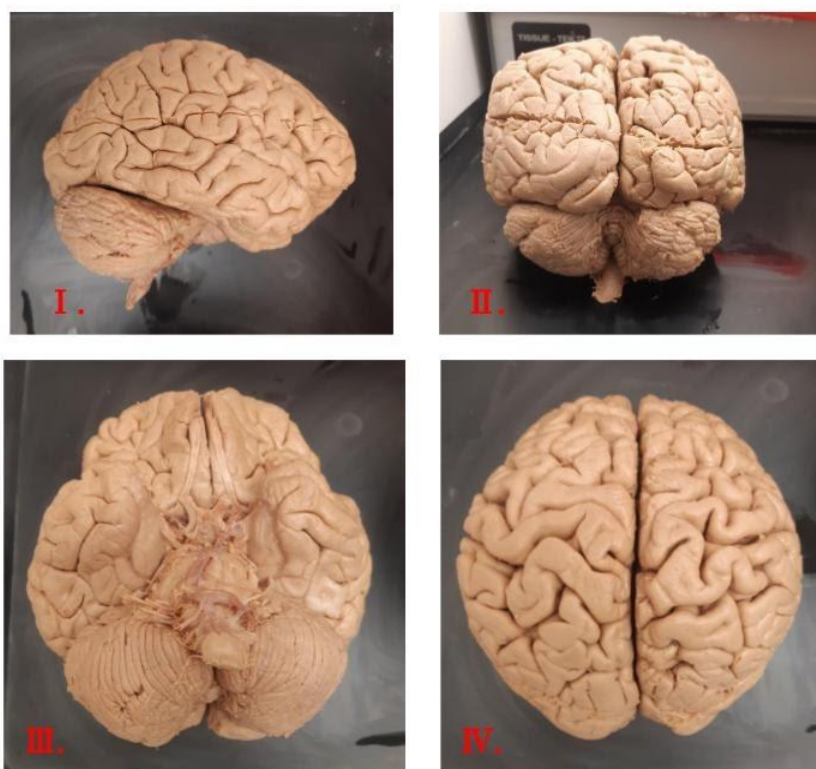


Figure 6. One post-mortem human brain specimen with the dura and pia mater removed from its surface. I. Lateral view II. Posterior view III. Ventral view IV. Dorsal view.

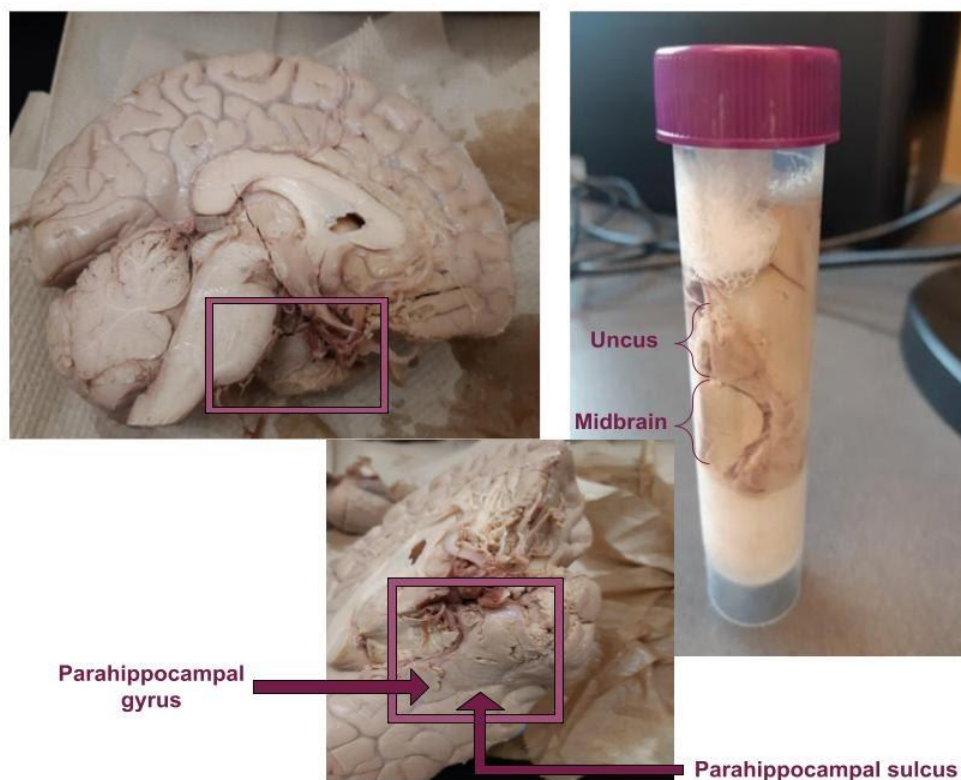


Figure 7. A resection of a left hemisphere MTL centered on the amygdala region (bounding box) placed in a plastic 2.5 cm cylindrical container fit for the 60 mm bore at the 9.4T MRI scanner.

2.3 MRI acquisition and pre-processing

The ten post-mortem human brain specimens (seven male and three female) donated to University Hospital were scanned at the Centre for Functional and Metabolic Mapping (CFMM) MRI suite at Robarts Research Institute located in London, Ontario, Canada. The whole-brain specimens were first scanned in their entirety in the custom 3D-printed container at the 7T MRI (Siemens MRI Plus). Specimens were dissected into their medial temporal lobe sections containing the amygdala prior to being scanned at 9.4T MRI (Bruker Biospec Avance III). The scanning sequences used for registration and segmentation were a T2-weighted SPACE MRI scan (TR = 4 msec; TE = 0.4 msec; flip

angle = 120°) acquired with a 1 mm³ isotropic resolution at 7T, and a T2-weighted TurboRARE MRI scan (TE=30 msec; TR=30 msec; flip angle = 90°) with 30 averages acquired at 9.4T at 0.1x0.1x0.2mm³ resolution. The slice thickness remained at 0.2mm rather than an isotropic 0.1mm due to limitations of the 9.4T scanner. The whole brain specimens were imaged at 7T for one hour each while each 9.4T amygdala prosection was scanned overnight for nine and a half hours each. The whole brain scans were registered to the standardized MNI ICBM Nonlinear 2009c Asymmetric template (<https://www.bic.mni.mcgill.ca/ServicesAtlases/ICBM152NLin2009>). Pre-processing of the T2-weighted anatomical scans included alignment, averaging, and resampling of the 9.4T amygdala images to 0.05mm³ resolution. ITK-SNAP was used to manually segment the 9.4T scans⁵⁹.

2.4 Manual registration of 9.4T MRI onto 7T MRI

Once the 1.0 mm³ isotropic whole brain *ex vivo* specimen scans were automatically registered to the MNI ICBM Nonlinear 2009c Asymmetric template using FSL's FLIRT pipeline, the 9.4T amygdala high resolution scans in their native space could be manually registered onto their corresponding anatomical locations on the whole brain 7T images using a program called 3D Slicer, permitting more accurate registration⁵⁸. First, the amygdala scans were corrected for RAI orientation to match those of their corresponding 7T whole brain scans. For all cases, the reoriented 9.4T image saw the axial viewpoint of the amygdala in the top left panel, the sagittal viewpoint in the top right, and the coronal viewpoint in the bottom right of the ITK-Snap windows prior to loading it into 3D Slicer for the manual registration process.

The Landmark Registration module in 3D Slicer (v.4.8.1) was used to register the 9.4T amygdala scan onto its correct corresponding location on the standardized whole brain 7T scan from which it was dissected. The 9.4T scan acted as the moving image represented on the bottom 3DSlicer panels while the fixed image represented by the 7T whole brain image placed on the upper panels. Four anatomical fiducials were chosen for all cases (Figures 8-11). The first anatomical fiducial is placed at the appearance of the lateral nucleus in the coronal view (Figure 8). The second anatomical fiducial is the most interior point of the inferior horn of the lateral ventricle at the most prominent uncal

emergence (Figure 9). The last brain slice of the uncus in the sagittal plane before its disappearance at the level of the hippocampal head represents the third fiducial marker (Figure 10). The last fiducial was placed in the centre of the hippocampal head at the level of the disappearance of the central nucleus of the amygdala (Figure 11). The placement of these four anatomical fiducials aids in the registration process for the 9.4T registration onto 7T MRI but also becomes a vital resource in the amygdala segmentation protocol.

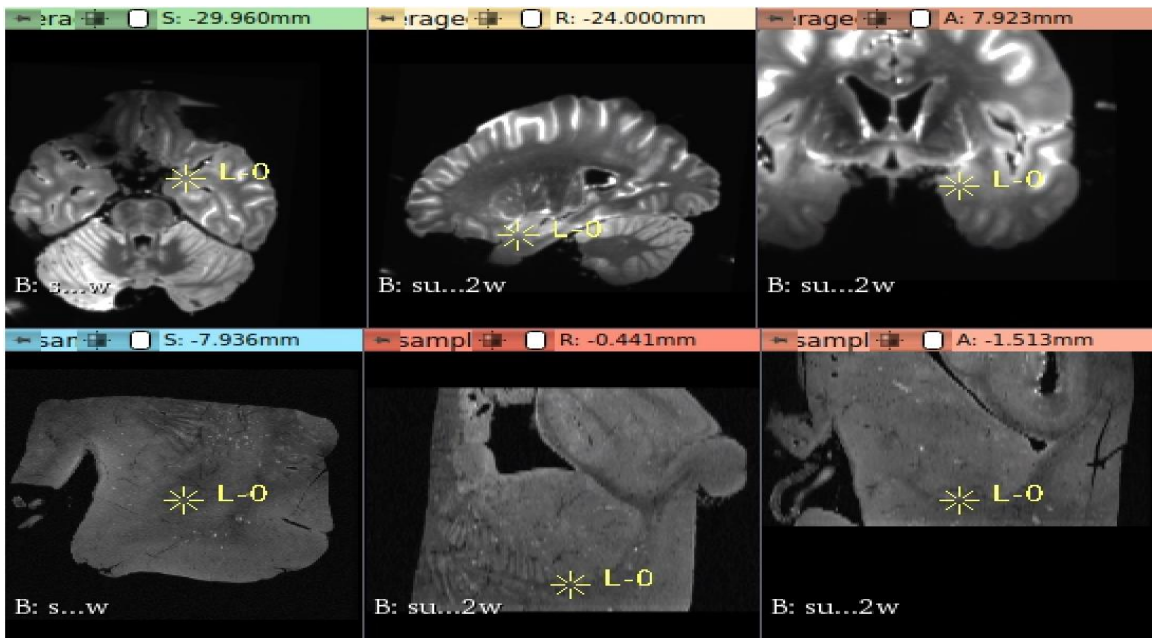


Figure 8. 9.4T to 7T MRI registration step one. The first fiducial represented by L-0 sits at the first slice of the lateral amygdala nucleus in the bottom left hand plane.

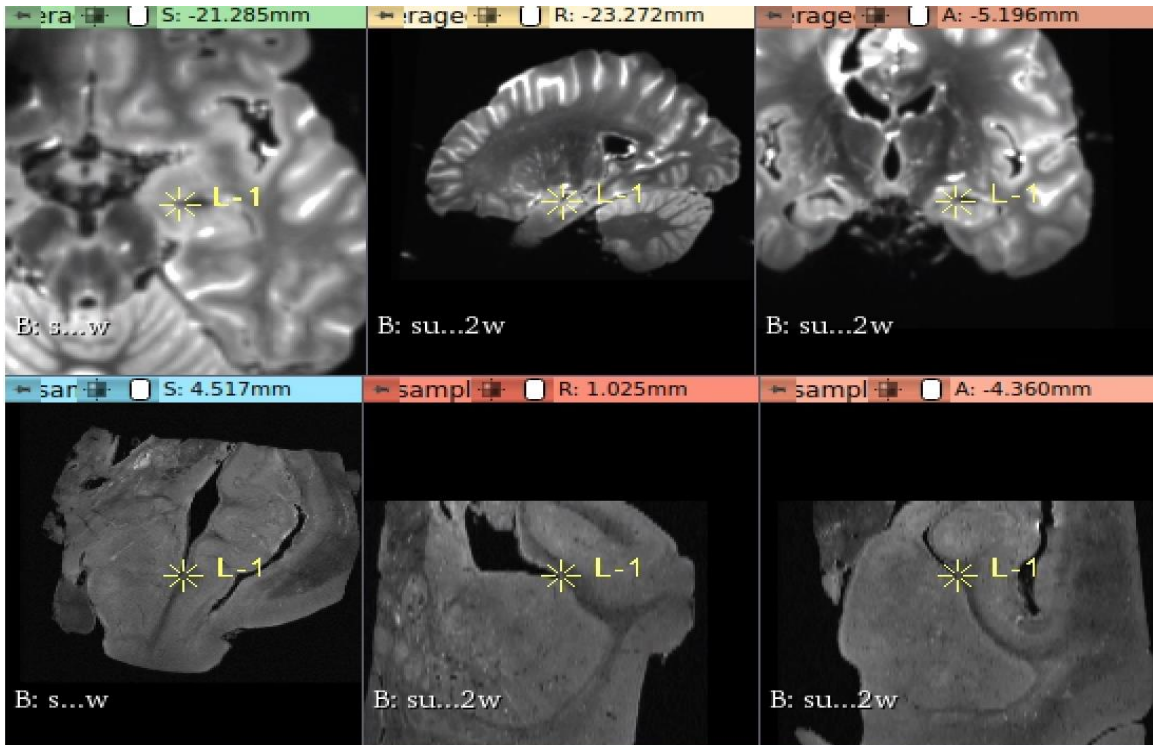


Figure 9. Step two of the 9.4T to 7T MRI registration. The L-1 fiducial represents the inferior horn of the lateral ventricle at the highest level of uncus prominence.

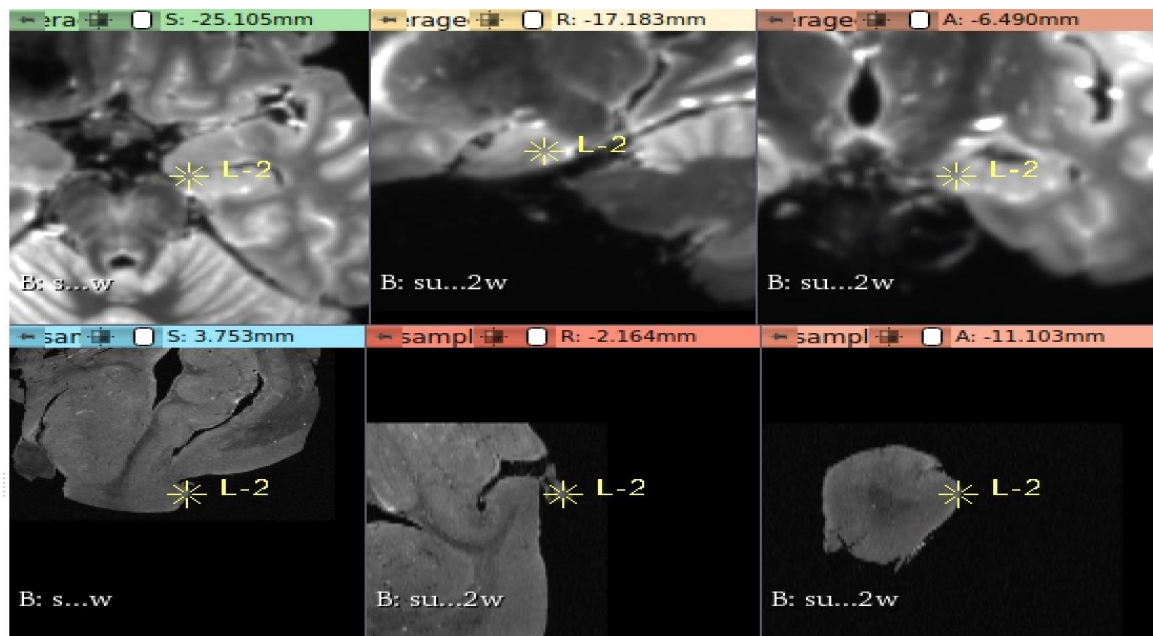


Figure 10. Step three of the 9.4T to 7T MRI registration. The L-2 fiducial represents the last slice of the uncus as observed in the lower middle sagittal 9.4T brain slice.

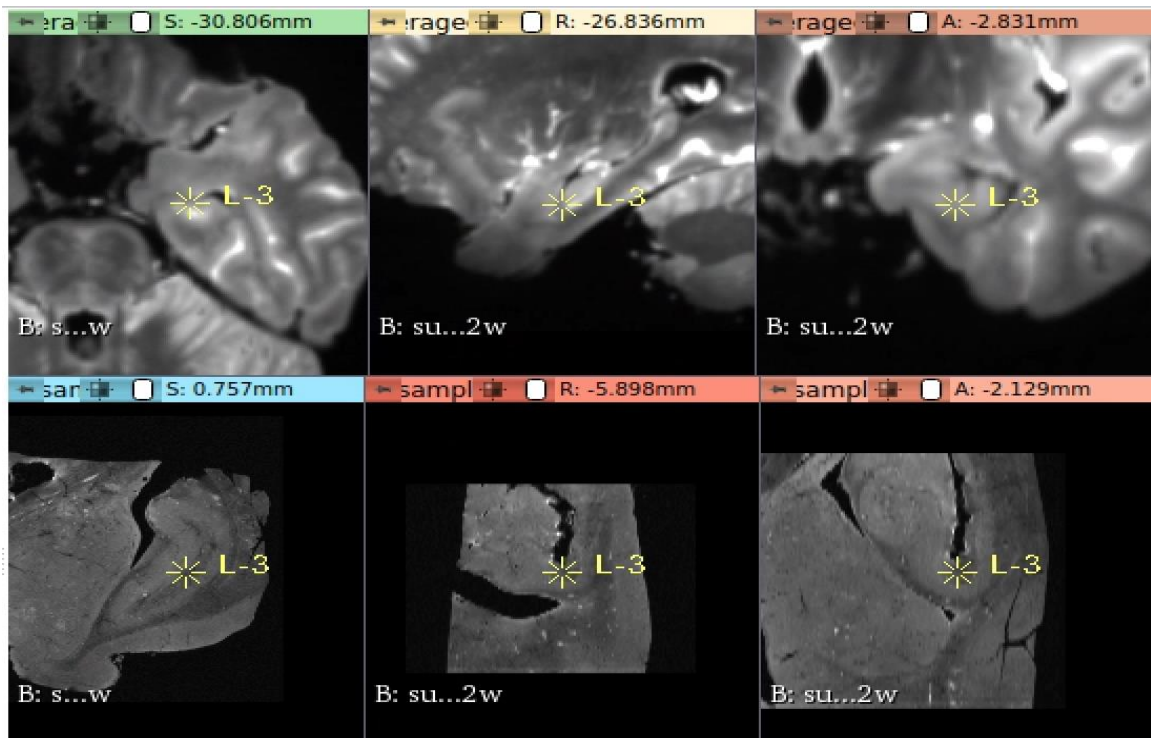


Figure 11. The 9.4T amygdala scan registered with the fourth anatomical fiducial L-3 placed in the centre of the hippocampal head onto its corresponding location on the 7T scan.

2.5 Target registration error (TRE)

The landmark registration fiducials placed on both the 7T acquired whole brain specimen and 9.4T amygdala only scan data using 3DSlicer can be quantified for their accuracy. There were four strategic fiducials placed on both scans of each specimen for each hemisphere ensuring the native 9.4T amygdala images were in rigid alignment with their correct positions on their corresponding whole brain specimens from which they were derived. A target registration error (TRE) is the distance between corresponding points, in this case between each of the four 7T and 9.4T landmark fiducials placed during registration⁶⁰. TRE is an error measurement that represents the Euclidean distance between two placed fiducials. Since MRI images are three-dimensional, there can be a TRE for each of the x, y, and z anatomical planes. The smaller the TRE, lower the error, thus signifying better registration. The TRE measurements were not used to drive the registration but instead were relied upon as a measure of registration accuracy.

2.6 Manual segmentation of the 9.4T MRI amygdala

Manual segmentation can begin following image post-processing and the registration of the 9.4T MRI amygdala scans onto their corresponding anatomical fiducial markers on their derived whole brain specimens imaged at 7T. ITK-SNAP is used to upload the registered 9.4T scans with a field of view (FOV) of the human amygdala for the purpose of parcellating its subnuclei. Segmentation is performed on a slice-by-slice basis using ITK-SNAP's polygon tool while viewing the horizontal, sagittal, and coronal image planes. A nucleus may visually appear more prominent in one view than another. Most segmentation steps occur in the coronal plane as that was the main plane in which MRI scanning pulse acquisition took place and as such unveiled higher resolution images. The manual segmentation protocol for the amygdala subnuclei is based upon Duvernoy's second edition 'The Human Brain: Surface, Three-Dimensional Sectional Anatomy with MRI, and Blood Supply' and Di Marino, Etienne, and Niddam's 'The Amygdaloid Nuclear Complex' neuroanatomy texts^{13, 64}. These instructions are general for the left or right hemisphere segmentations. One MRI slice in which the amygdala subnuclei were segmented on the 9.4T image in reference to its 7T whole brain scan is displayed as an overview (Figure 21). The step-by-step nature of the manual segmentation protocol is typically outlined in an anterior to posterior manner (Figure 22). It is recommended that the 9 amygdala subnuclei are parcellated in the following order.

2.6.1 Paralaminar nucleus

The paralaminar (PL) nucleus is the most inferiorly localized amygdala subnucleus (Figure 12). It is anatomically closest to the head of the hippocampus. In a way, the PL follows the outline of hippocampal head shape with regards to its digitations or bumps. This nucleus is distinct from the others because it appears in a thin band that is darker in contrast compared to the rest of the amygdala subnuclei. This darker outline is thought to be representative of the underlying histology. Neuronal cell bodies are most densely packed in the PL nucleus region. Sometimes the band remains dark to the absolute inferior edge of the amygdala but sometimes the band is visible while underneath it the image contrast remains similar to the other nuclei. Once the thin darker band is observed, the segmentation for the PL nucleus can take place along the PL nucleus line as well as

below it. It is best to start the parcellation of the PL nucleus at the posterior end of the amygdala. This makes it easier to notice the end of the PL nucleus at the anterior end where the BLA commences. The PL nucleus is present in about half of all amygdala slices.

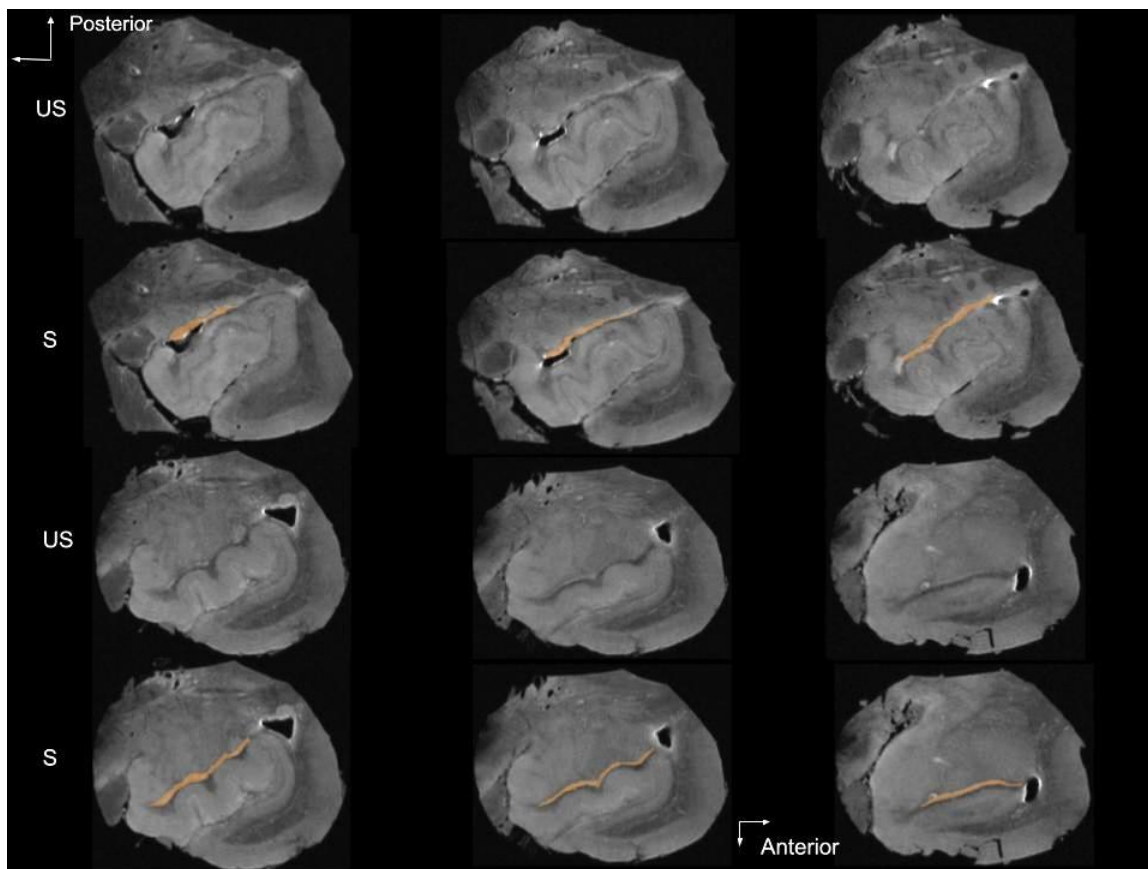


Figure 12. Segmentation of the left PL nucleus (coronal plane) from posterior to anterior. US = Unsegmented, S = Segmented.

2.6.2 Lateral nucleus

The lateral nucleus of the amygdala is one of the first nuclei to appear at the anterior beginning of the structure (Figure 13). Start by scrolling anteriorly in the coronal plane from the posterior end where the hippocampal head is visible. The amygdala is located superiorly to the hippocampus at the inferior horn of the lateral ventricle juncture. It is the most laterally located amygdala subnucleus, furthest away from the medial brain midline where the uncus is found. At the most anterior end, it is the first nucleus to appear as a small round grey matter point against the darker white matter fibers it surrounds. In the

next few posterior slices, the emergence of the neighbouring basolateral nucleus of the BLA will be evident by a slim darker white matter separation, especially towards their superior end. The lateral nucleus is one of the more recognizable amygdala nuclei because of its striated appearance usually in its upper half. These striations represent myelinated neuronal fibers innervations related to the connections the amygdala has with the neocortex. Moving posteriorly, the lateral nucleus can be segmented in almost every slice of the amygdala. There will be a point at the very posterior of the amygdala where the lateral amygdala ends and the basolateral nucleus takes predominance for the last slices of the entire structure.

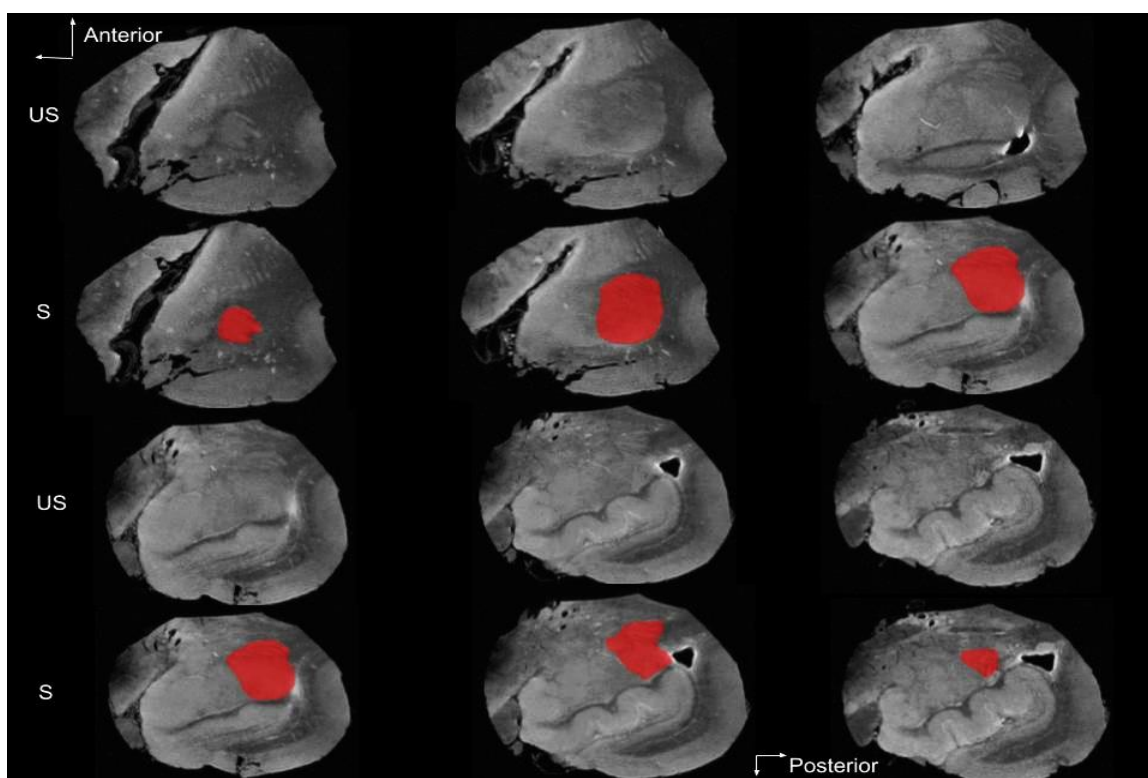


Figure 13. Segmentation of the left lateral amygdala subnucleus (coronal plane) from anterior to posterior. US = Unsegmented, S = Segmented.

2.6.3 Basolateral nucleus

The basolateral nucleus of the amygdala borders the lateral nucleus throughout the span of the amygdala (Figure 14). After the lateral nucleus is segmented completely, begin segmentation of the basolateral nucleus again starting at the anterior end of the amygdala. This nucleus will also first appear as a small round grey matter piece at its origination.

The basomedial nucleus borders the basolateral nucleus on its medial side with a thin white matter darker coloured band cleaving the two nuclei more noticeably near the top. Oftentimes, the cleaved white matter separation can be observed splitting the BLA nuclei completely, it is simply more difficult to make out towards the inferior closer to the hippocampal head. There may be a portion of the inferior basolateral nucleus that extends medially towards the direction of the uncus to meet the CATA. The basomedial nucleus in these instances may also be superior to not only medially located in reference to the basolateral nucleus.

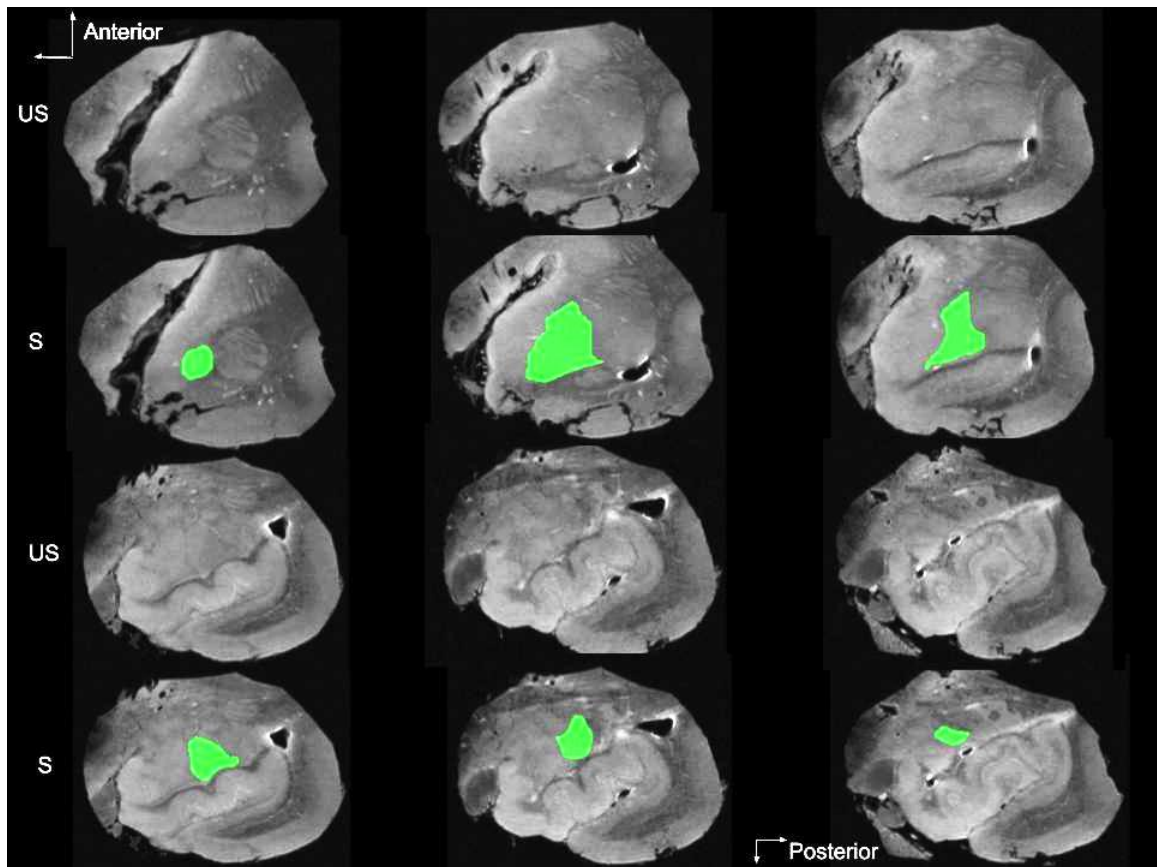


Figure 14. Segmentation of the left basolateral subnucleus (coronal plane) from anterior to posterior. US = Unsegmented, S = Segmented.

2.6.4 Basomedial nucleus

Like the other subnucleimembers of the BLA, it is easiest to commence parcellating the basomedial from the amygdala's anterior end. After the lateral and basolateral nuclei are segmented, the next most medial nucleus bordering them is the basomedial nucleus. The

basomedial nucleus is most often oval in shape. The CATA is the most medial amygdala subnucleus and it rests lateral to the basomedial nucleus following the curvature of the uncus. The basomedial nucleus can be distinguished from the CATA because it appears brighter in the acquired T2-weighted images in comparison to its member BLA nuclei. Again, there is a slight white matter innervation appearing darker grey that cleaves the superior end of the basomedial nucleus apart from the CATA (Figure 15). The central and medial amygdala nuclei are found directly above the basomedial nucleus about halfway through the total slices within the amygdala.

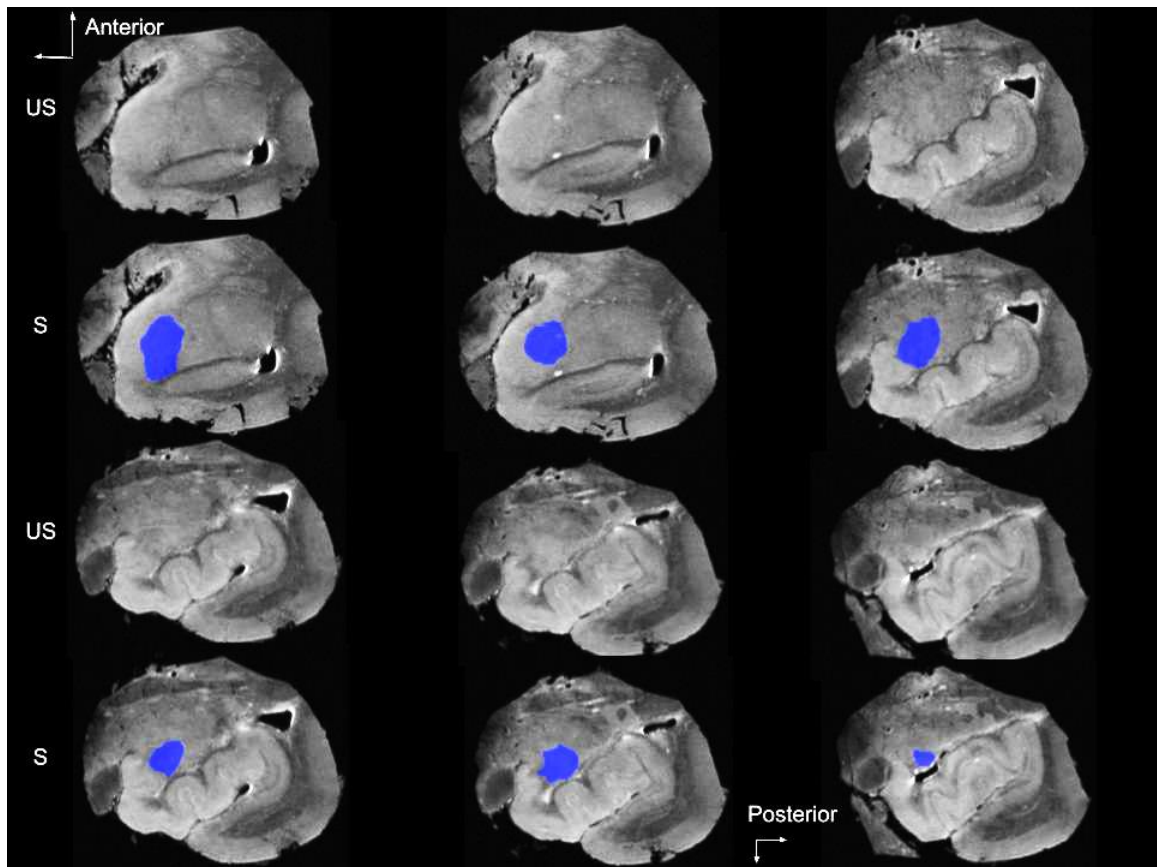


Figure 15. Segmentation of the left basomedial subnucleus (coronal plane) from anterior to posterior. US = Unsegmented, S = Segmented.

2.6.5 Corticoamygdaloid transition area (CATA)

The CATA is the most medially located nucleus of the amygdala (Figure 16). It follows the curvature of the uncus around its apex. This nucleus may have a similar neuronal density as the amygdaloid hippocampal transition area and the hippocampal head as

proxied by similar image contrast. The shape of the CATA is similar to that of a jellybean. It is present throughout most slices of the amygdala from anterior to posterior. It is one of the last subnuclei visible to be segmented at the posterior end, and it is recommended that parcellation begins here. As the BLA nuclei will have already been segmented, it will be easier to outline the CATA at the most medial side of the amygdala, continuous with the uncus and similar in contrast with the transition of the hippocampal head. The first slices of the CATA at the anterior end of the amygdala begin when the last slices of the anterior amygdala area (AAA) end.

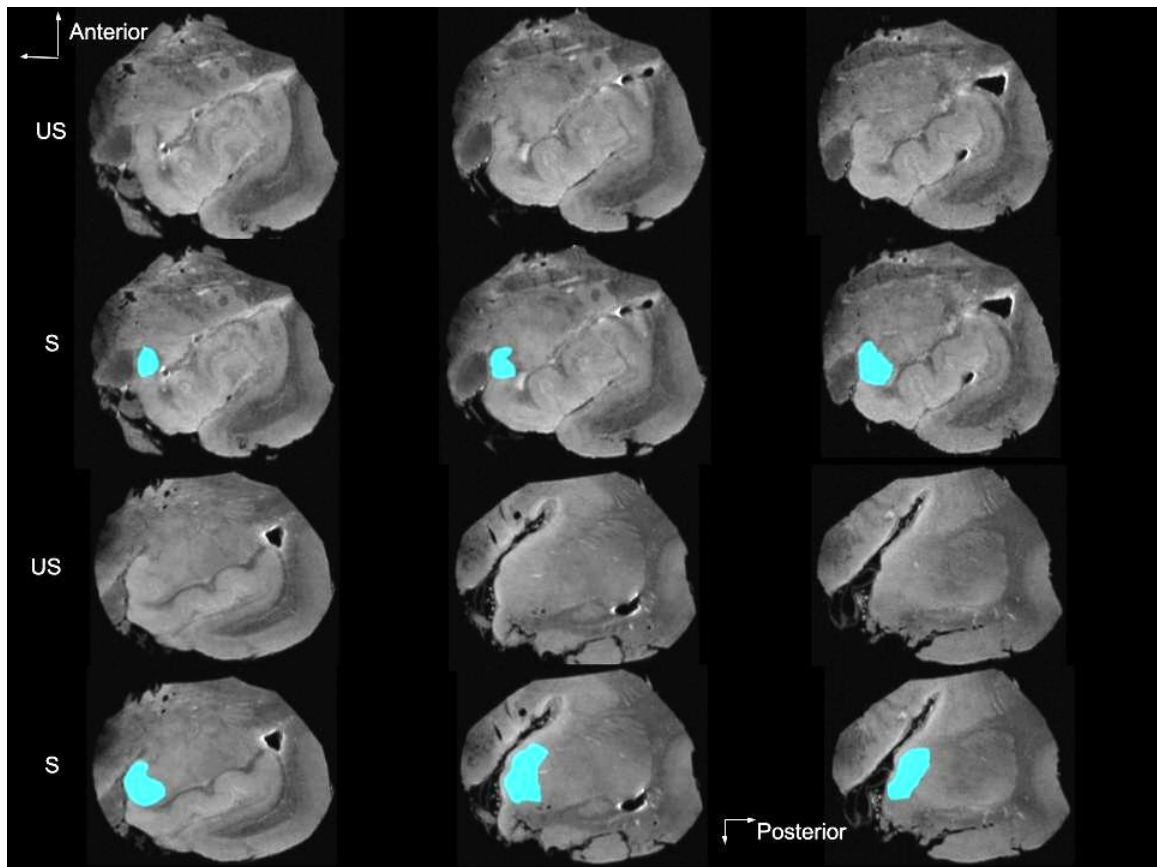


Figure 16. Segmentation of the left CATA (coronal plane) from posterior to anterior. US = Unsegmented, S = Segmented.

2.6.6 Central nucleus

The central nucleus of the amygdala finds itself amongst the middle MRI slices of the structure. It is one of the smallest amygdala nuclei and it is overall often oval shaped. It stands above and apart from the already segmented inferior nuclei, the BLA, CATA, and

PL nuclei. In particular, it rests above the basolateral and basomedial nuclei, and it lies lateral to the medial nucleus. It is suggested the segmentation of the central nucleus begins from the anterior amygdala end because it is trickier to determine its termination towards the posterior end. The central nucleus can be made out because it stands as an island surrounded by slightly darker contrast white matter on T2-weighted images (Figure 17). It does not appear prior to the formation of the basomedial or medial subnuclei from the anterior start. The ending slices to be segmented of the central nucleus occur before the disappearance of the lateral subnucleus at the posterior end.

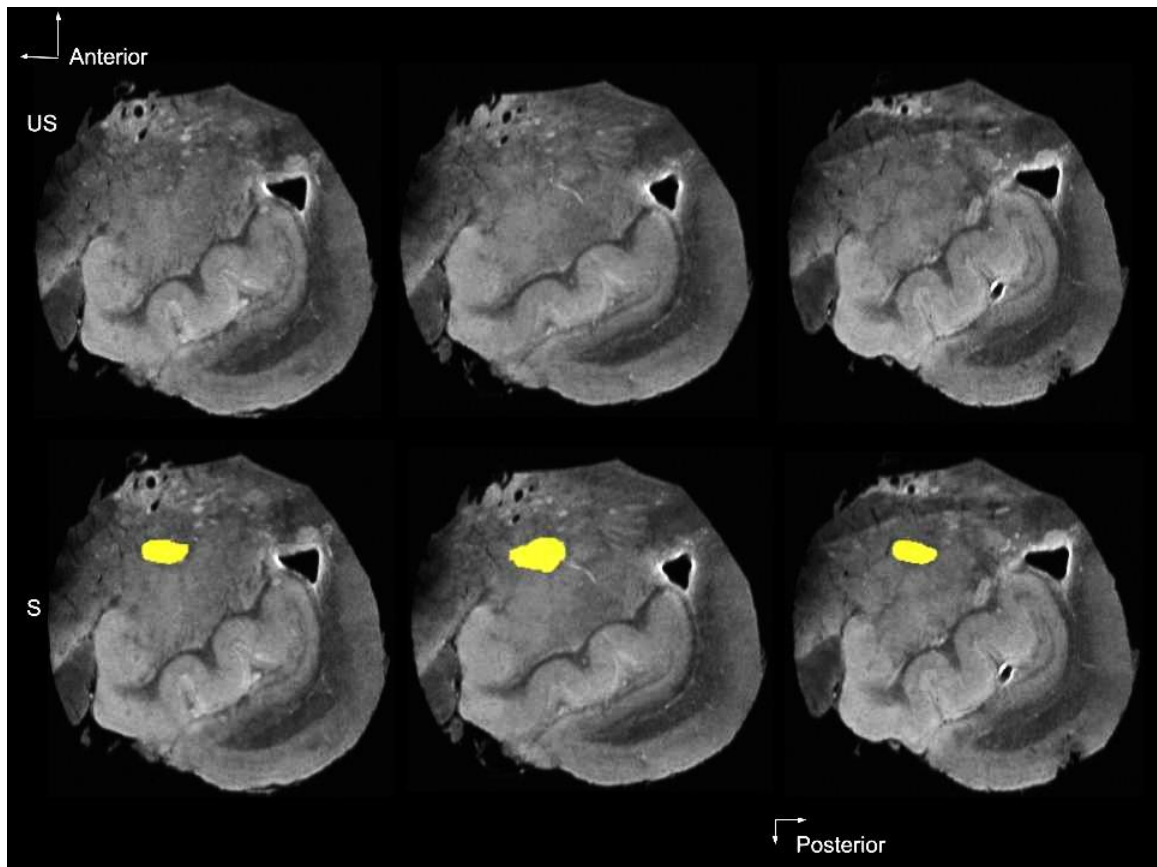


Figure 17. Left central amygdala nucleus segmentation (coronal plane) from anterior to posterior. US = Unsegmented, S = Segmented.

2.6.7 Medial nucleus

Since the central nucleus is often a more evident structure to segment, it helps if the parcellation of the medial nucleus follows that of the central nucleus. The medial and central nuclei are the two nuclei that are most similar to one another anatomically. They

are almost mirror images of one another, with the medial nucleus located more medially, closer to the uncus. The medial nucleus, like the central nucleus, is small and roundly shaped. It too is present within the middle portion of the amygdala MRI slices on the 9.4T scans. It is adjacent to the central nucleus and can be clearly distinguished from the darker contrast white matter that surrounds it. Once slices from the head of the hippocampus appear, pay close attention to the region superior to the basolateral and basomedial subnuclei where the medial nucleus will emerge (Figure 18). One of the last slices of the medial nucleus to be segmented is around the time the lateral nucleus of the amygdala disappears.

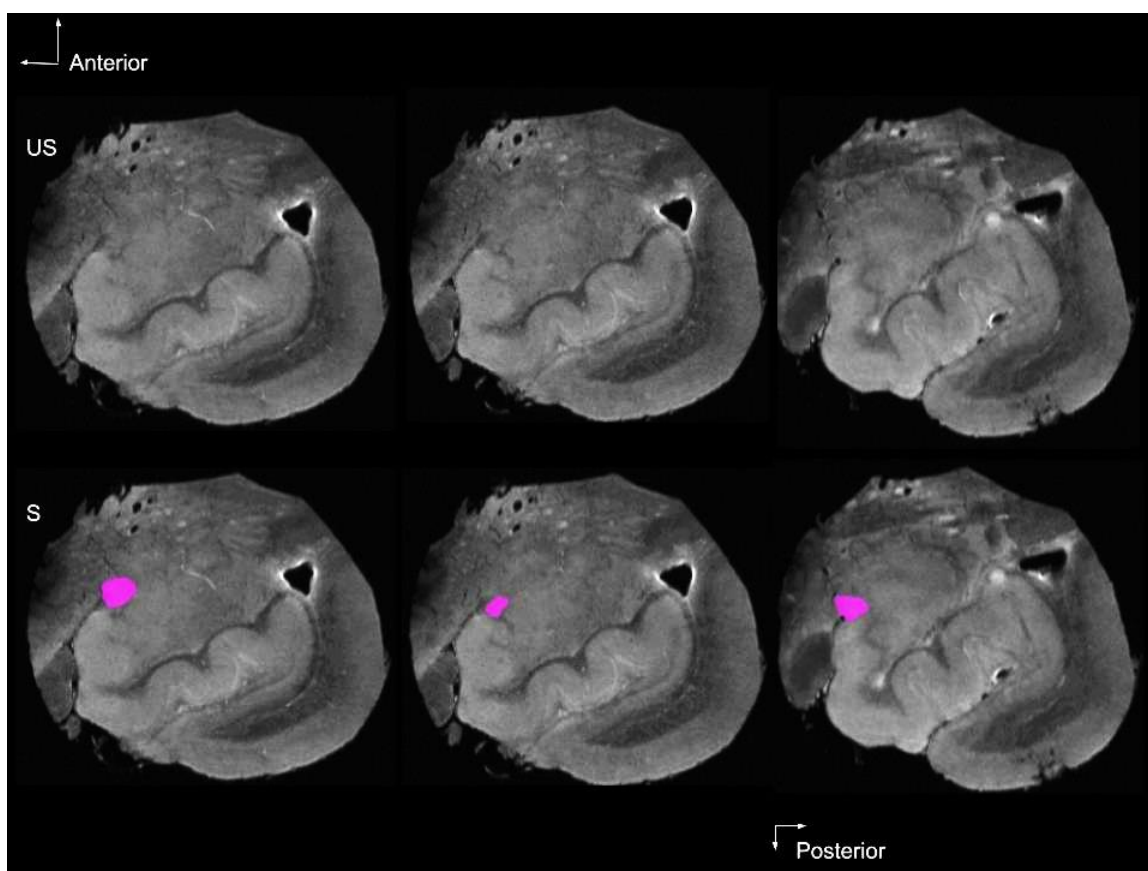


Figure 18. The left medial nucleus parcellated starting anteriorly on the left hand side. US = Unsegmented, S = Segmented.

2.6.8 Cortical nucleus

The smallest and most difficult to segment nucleus is the cortical subnucleus (Figure 19). It is circular in shape and it is wedged between the CATA and basomedial nucleus. Since

the basomedial and CATA nuclei will have already been segmented, the paintbrush tool will be used to segment over these subnuclei once you pinpoint the cortical nucleus location is pinpointed. The cortical nucleus will only be present in a few of the total MRI slices capturing the amygdala. This nucleus makes an appearance closer to the posterior end of the amygdala structure. It is most often detected at the superior break indent between the CATA and basomedial nucleus just inferior to the location of the medial subnucleus. Once the central and lateral nuclei disappear at the posterior end of the amygdala, so does the cortical nucleus.

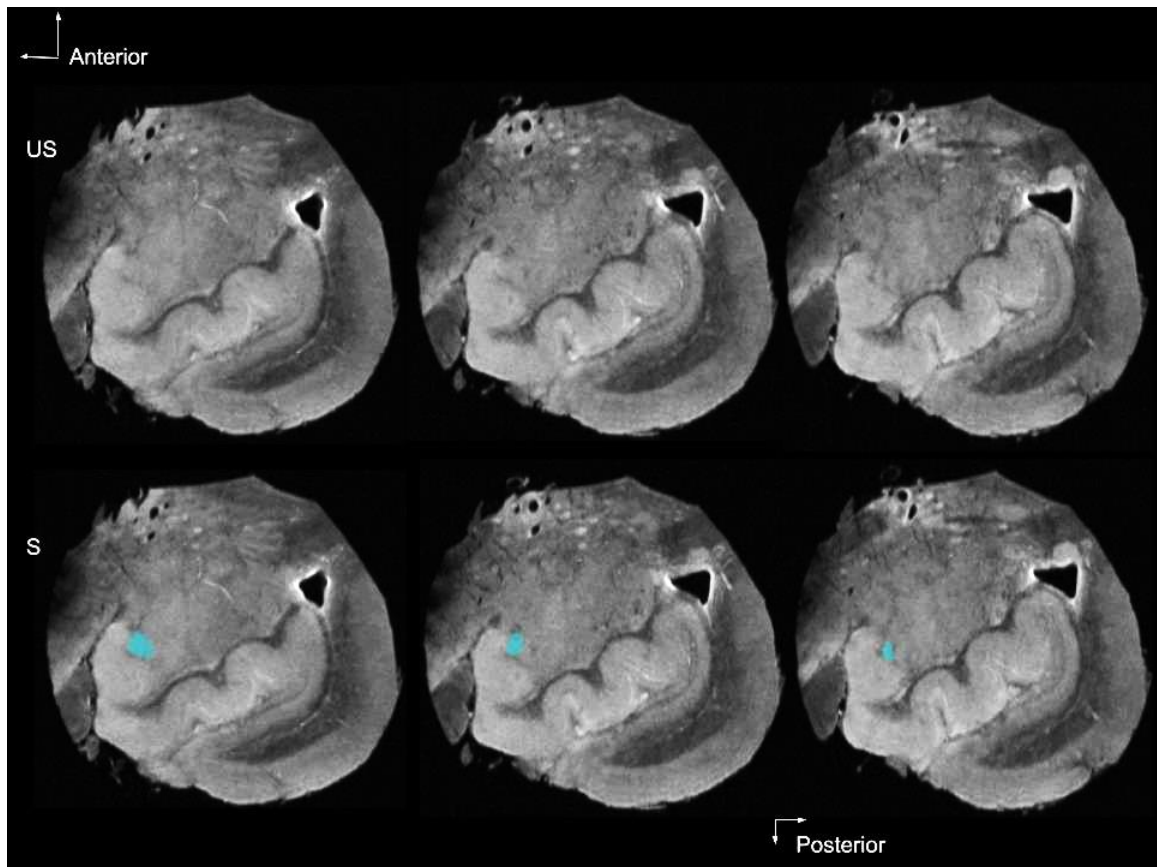


Figure 19. The amygdala's left cortical nucleus (coronal view) segmented from the anterior to posterior. US = Unsegmented, S = Segmented.

2.6.9 Anterior amygdala area (AAA)

The anterior amygdala area (AAA) is the most superiorly and anteriorly situated amygdala subnucleus (Figure 20). It is the first subnucleus to appear at the anterior end and it is often shaped like a frisbee when viewed from the side in the coronal plane. The

AAA lies oblique to the cortex on its medial side. Sometimes but not always, the AAA exhibits the striated pattern of white matter tracts running through the grey matter nucleus similar to that of the upper lateral nucleus. It typically presents superior to the lateral nucleus, barred by a section of darker image contrast representing the white matter separating the two grey matter subnuclei. The AAA is displayed only in the first few amygdala MRI slices from the anterior end. This nucleus ceases to be visible following the appearance of the basomedial nucleus.

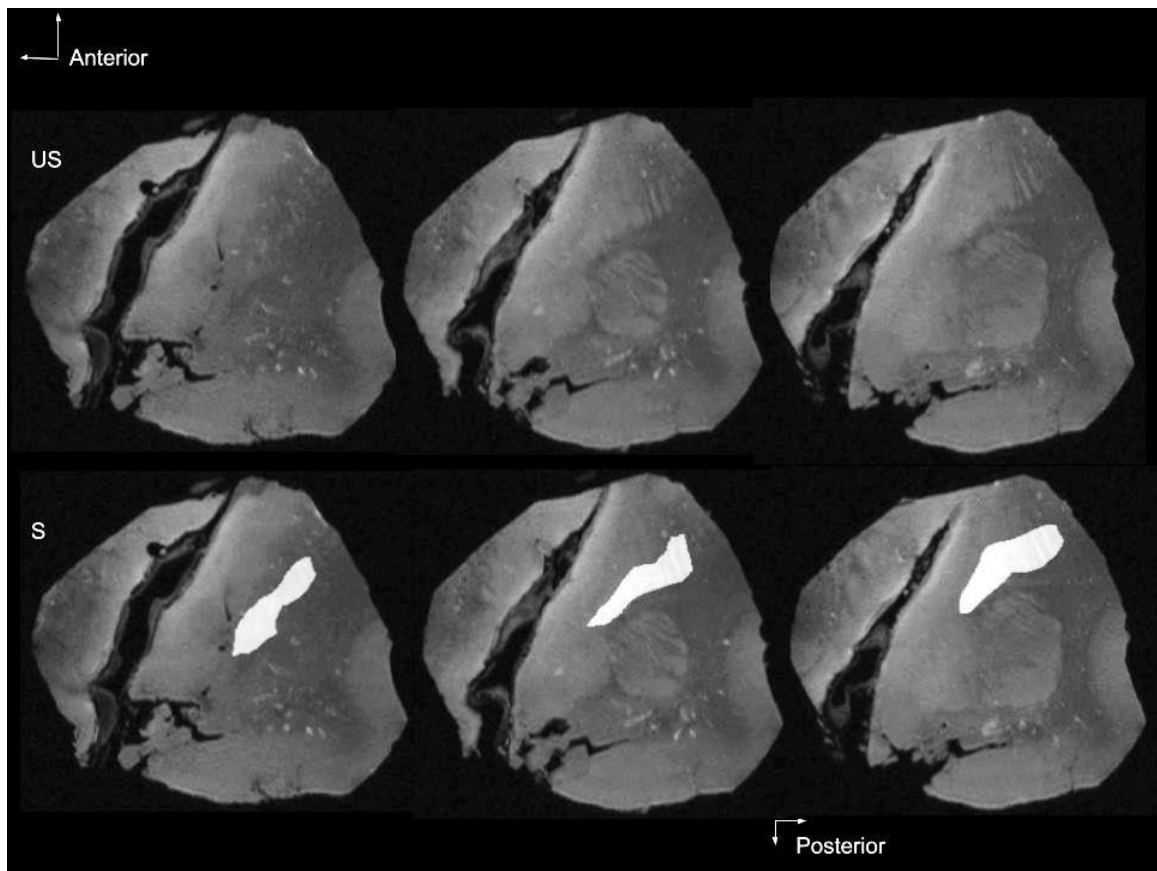


Figure 20. The AAA parcellated at the left amygdala's anterior end. US = Unsegmented, S = Segmented.

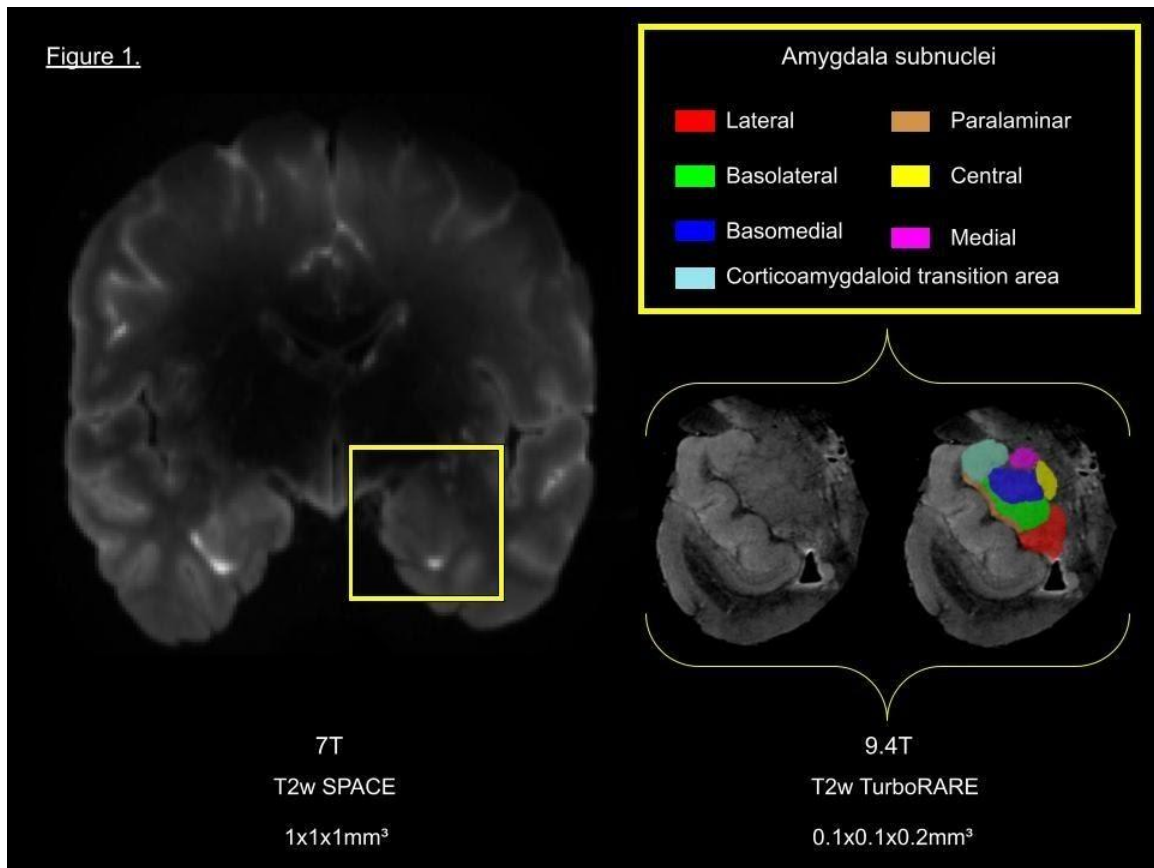


Figure 21. The 9.4T high resolution scans (bottom right) outlined in reference to the 7T whole brain ex vivo specimens (left) from which they were derived. The legend (top right) includes the coloured-labelling for seven out of nine visible amygdala subnuclei.

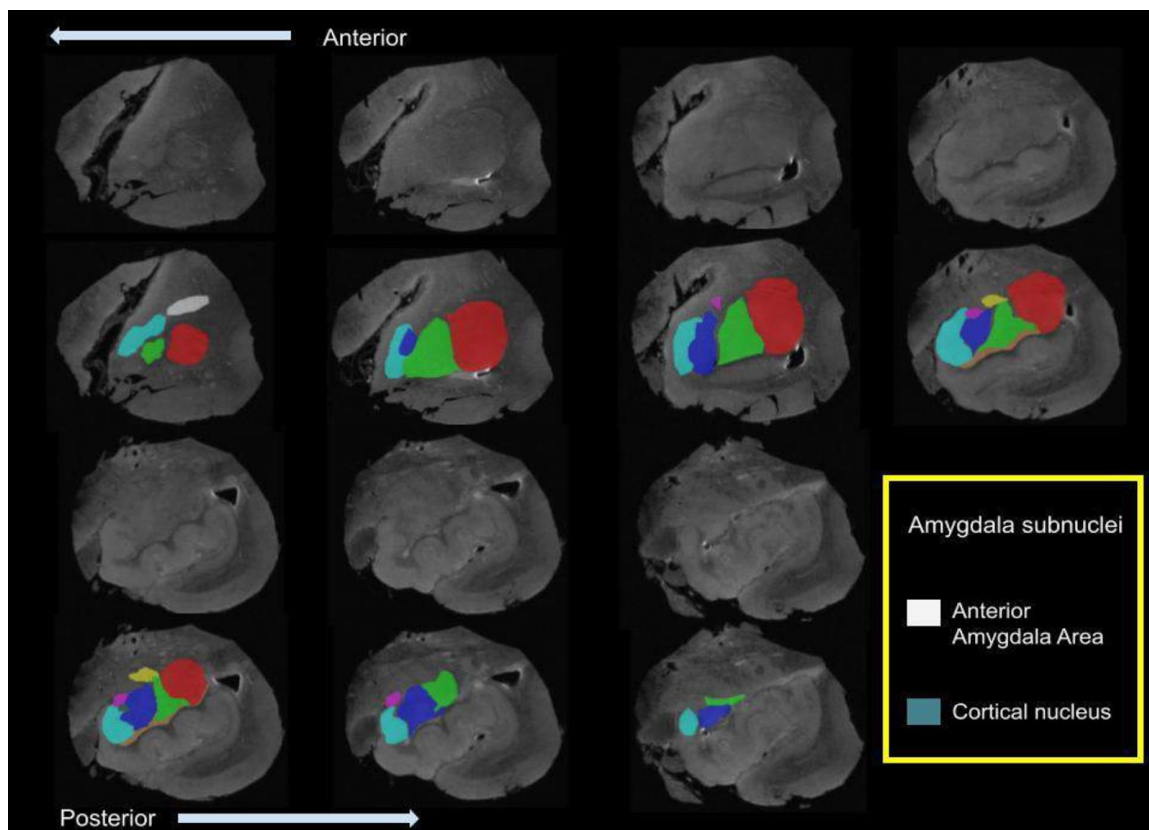


Figure 22. The amygdala subnuclei segmented from the anterior end at the top left to the posterior end at the bottom right. The first and third rows represent the registered MRI images through some representative amygdala slices while the second and fourth rows represent their respective parcellated amygdala subnuclei slices. The amygdala subnuclei legend here is continued from Figure 21.

2.7 Ultra-high-resolution MRI and histology public datasets (BigBrain and Edlow)

In addition to the acquisition of the *ex vivo* whole brain and amygdala prosection MRI scans in the current study, another aim of the work is applying the manual amygdala segmentation protocol to two ultra-high resolution MRI and histology datasets with an overlaid amygdala subnuclei automated atlas as a comparison. While we obtained some high-resolution amygdala focused images from the 9.4T scans, there are still difficulties in outlining some substructure boundaries which may potentially be solved when observing high resolution MRI scans acquired over a longer period of time or histological data available with finer molecular detail.

Edlow and colleagues were able to use a high magnetic field strength 7T scanner to image a post-mortem 58-year old female human brain specimen⁷⁴. With over 100 hours of combined scanning time at 100 μm resolution this dataset provides an unprecedented view of the 3D neuroanatomy of the human brain. The whole brain *ex vivo* specimens in the current study were scanned for only one hour at 1000 μm resolution.

BigBrain is an ultra-high-resolution histological dataset of a 65-year-old male post-mortem specimen who passed away without any brain pathology⁷⁵. This specimen was scanned using MRI before it was sliced into 7,404 sections using a microtome. The brain slices were stained for cell bodies using the Merker method where darkly stained areas represent grey matter and uncoloured areas signify the white matter of the brain's tissue⁷⁸. The result is a 3D whole brain atlas with a fine 20 μm spatial resolution. In the present study, the amygdala specific 9.4T scans were obtained at an in-plane resolution of 100 μm before resampling to 50 μm . A starting isotropic 20 μm spatial resolution obtained from BigBrain includes a thinner slice thickness which may make a significant difference in the ability to resolve small structures and boundaries.

Both free publicly available datasets were downloaded in order to investigate the anatomy of amygdala subnuclei with the highest resolution MRI and histological data obtainable. The BigBrain amygdalohippocampal region at 100 μm resolution was used, matching the 100 μm resolution MRI from the Edlow study. The Edlow post-mortem specimen data pulled was already registered to the standard MNI ICBM 2009a nonlinear asymmetrical template ensuring segmented volumes would be comparable. Using the 3D Slicer program, the BigBrain temporal lobe portion with the amygdala structure in mind was registered to the amygdala region in Edlow's MRI to ensure it was in the same spatial location. The amygdala subnuclei segmentation protocol of the current study was followed for each of the MRI and histological modalities. The number of and name of the amygdala subnuclei are the same between the present protocol and the protocol accompanying the Saygin Freesurfer pipeline. This work will run Saygin's Freesurfer 7.1 amygdala subnuclei atlas pipeline on these data to compare the accuracy of their labelling in automated and manually segmented high resolution cases by rater SP (Figure 23)⁵⁵.

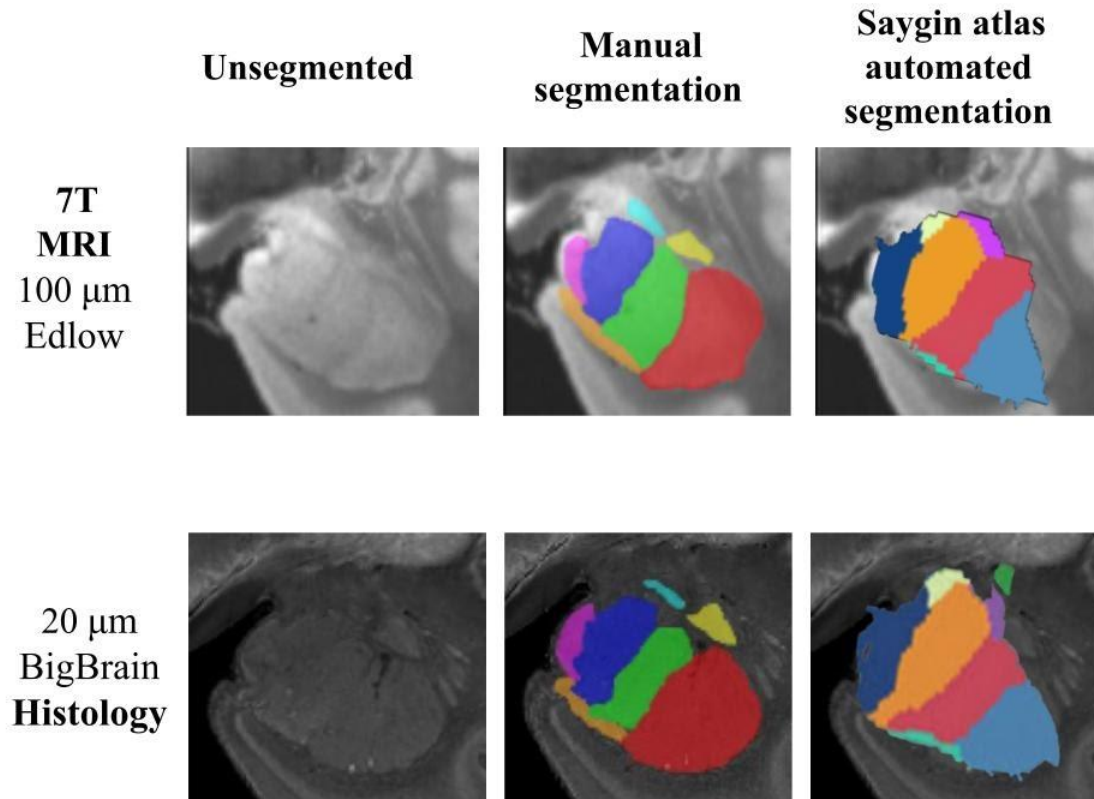


Figure 23. A slice through the left human amygdala unsegmented, manually segmented, and automatically segmented from ultra-high resolution MRI and histology data.

2.8 Reliability measures

The manual segmentation protocol of the nine amygdala subnuclei previously described may be verified using reliability measures. One such measure is intra-rater reliability. Intra-rater reliability is conducted when a segmentation protocol is completed twice at different instances in time by the same user. This measure determines how well the same individual can follow the same protocol. SP segmented all nine amygdala subnuclei for 20 amygdala specific scans from 10 post-mortem specimens using the protocol previously described. Then, after a period of 4 to 6 weeks following the initial segmentations, SP segmented all amygdala subnuclei for all the scans a second time. All subnuclei were given a label and compared in terms of the first and second parcellations completed by the same rater, SP, computing the intra-rater reliability. A second rater,

DC segmented 6 amygdala specific 9.4T scans from three *ex vivo* whole brain specimen scans. DC's scans were compared to the same specimen's segmented images by SP's first instance to denote inter-rater reliability. The inter-rater reliability measure determines how well two raters parcellate substructures following the same protocol.

The dice similarity coefficient is the method used to compute intra and inter-rater reliabilities. This measure is used in manual segmentation protocols and methodological studies. The dice similarity coefficient is a spatial overlap that validates medical volume segmentations⁶¹. It measures the repeatability and reproducibility of manual segmentations such as the amygdala subnuclei parcellated here. The equation is as follows:

$$\text{Dice similarity coefficient} = 2(a \cap b)/a + b$$

Whereby a represents the number of voxels unique to one segmentation and b the number of voxels unique to the other segmentation⁶². In the case of intra-rater reliability, a and b are the segmentations performed by the same rater SP at two different instances in time while for the inter-rater reliability measure, a and b are the comparisons between the segmentations completed by the two different raters SP and DC. The dice similarity coefficient score results in a range from 0 to 1. A coefficient score of 0 means there would be no overlap between segmentations but a score closer to 1 would mean perfect overlap between parcellations. These scores are computed for all nine amygdala subnuclei labels separately.

One downside of the dice similarity coefficient is that regions small in shape are much more likely to see lower scores because most errors occur at segmentation boundaries. Smaller substructures are subjectively prone to segmentation border discrepancies. Another measure of the reliability of the manual segmentation protocol is the intraclass correlation coefficient (ICC). The ICC calculates the variance of a population (σ_b^2) in addition to the variance of the rater (σ_0^2)⁶³. This measure determines the ratio between the population of measurements and the variance of a normally distributed population.

The ICC equation is: $\rho = \sigma_b^2 / (\sigma_b^2 + \sigma_0^2)$

If the rater's variance value relative to the total ICC result is small, it suggests measurement variations among different cases may be due to a naturally occurring variance in the population in which case the value of the ICC would be close to 1. This would incur a high degree of confidence in the rater's segmentation reliability. Accepted ICC values range from 0.9 to 0.99 for manual tracing volume assessments in intra and inter-rater reliability neuroimaging applications. This score was computed with a program called JASP (<https://jasp-stats.org>). Both the dice similarity coefficient and intraclass correlation coefficients were determined for the comparison of the automatically segmented and manually segmented amygdala subnuclei in the 7T MRI and BigBrain histology datasets.

Chapter 3

3 Results

This section outlines the amygdala subnuclei volumetry results as well as the intra and inter-rater Dice similarity and intraclass correlation coefficients results following the completion of the manual segmentation protocol previously described. Prior to the segmentation results, the determinant of the registration process, the target registration error is presented.

3.1 Target Registration Error

In advance of the commencement of the manual segmentation protocol of the amygdala subnuclei, the 9.4T amygdala specific scans were rigidly registered onto their corresponding anatomical locations on their whole brain specimen counterparts scanned at 7T. Four landmark fiducial placement steps were adhered to in the registration process (2.4). Each fiducial has a TRE for the x, y, and z planes (Table 2). The TRE is measured in millimeters and the range of the values are included. The result of each anatomical plane TRE is an average of each fiducial point's TRE for all 20 total amygdala subnuclei registrations.

| | 1 | | | 2 | | | 3 | | | 4 | | |
|-----------------|---------|---------|---------|---------|---------|---------|---------|---------|---------|---------|---------|---------|
| | x | y | z | x | y | z | x | y | z | x | y | z |
| TRE in mm | 1.2 | 2.7 | 2.2 | 1.1 | 1.7 | 2.3 | 2.7 | 2.9 | 3.3 | 4.1 | 3.6 | 3.1 |
| TRE range in mm | 0.9-3.1 | 1.4-3.6 | 1.3-3.1 | 0.4-3.5 | 1.1-3.7 | 1.5-4.4 | 1.8-4.1 | 2.1-4.5 | 1.5-5.2 | 2.7-4.9 | 2.6-4.7 | 1.9-4.2 |

Table 2. The averaged and range of TRE values for the x, y, and z planes of four landmark fiducials (top row) used to register 20 amygdala subnuclei scans onto their whole brain specimen counterparts.

The TRE of all placed fiducials are generally low suggesting that the 9.4T amygdala specimens were rigidly registered well onto their whole brain specimen targets. The entire amygdala averages about 2 to 4cm in diameter. TRE ranges upwards of 5mm may

be considered moderately higher, especially when some amygdala subnuclei may be under a centimeter in diameter. Fiducials 1 and 2 have slightly lower TRE as they have clearer boundaries in regards to the lateral nucleus emergence at the anterior end and the inferior horn of the lateral ventricle. Fiducials 3 and 4 respectively representing the last slice of the uncus and the center of the hippocampal head have a slightly higher TRE compared to the first two fiduciary placements because there is greater individual variation between specimens in the localization of these areas. But overall, a recommended proposal using these four anatomical fiducials when registering MTL substructures like the amygdala or hippocampus would hold well in future applications.

3.2 Volume measurements of amygdala subnuclei

Following registration and the adherence of the manual segmentation protocol (Section 2.6), a resulting three-dimensional rendering of the amygdala and its substructures can be generated automatically by the ITK-SNAP software (Figure 24).

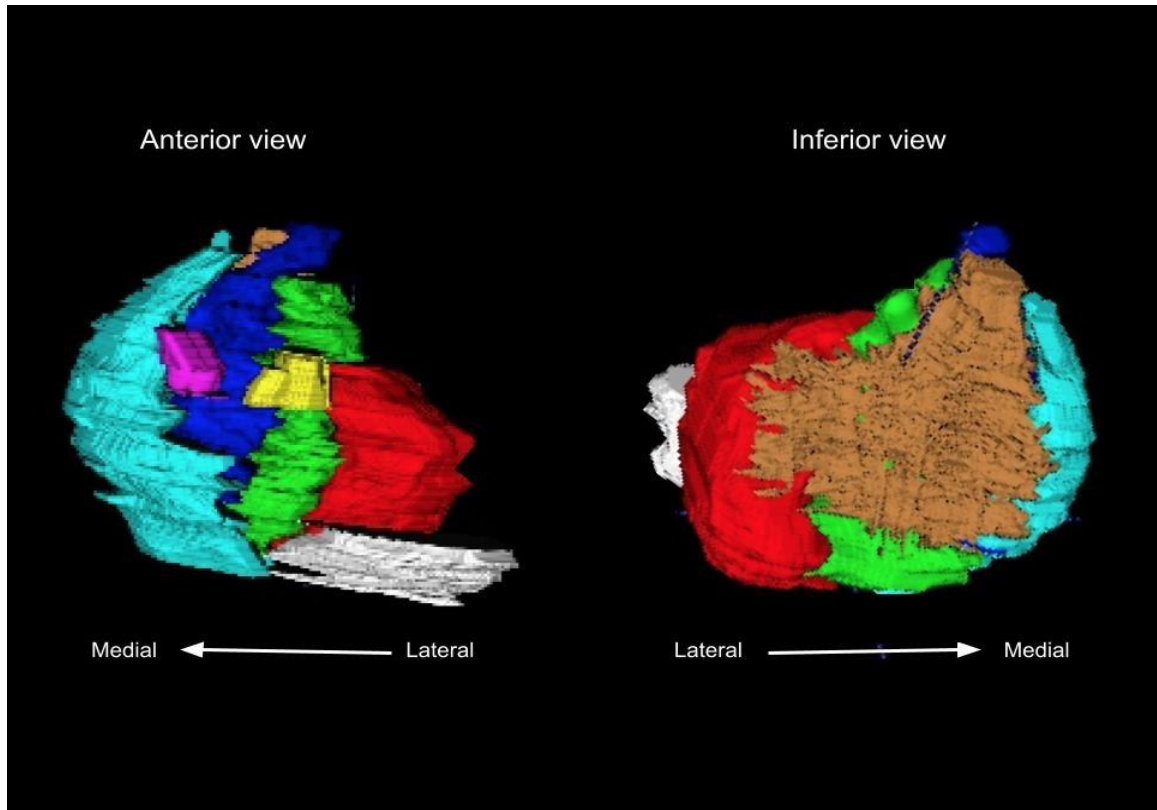


Figure 24. 3D rendering of the left amygdala and its substructures from anterior and inferior viewpoints. The legend for subnuclei can be found in Figures 21 and 22.

Volumetric measurements of the amygdala subnuclei are outputted directly by the visualization and segmentation program ITK-SNAP and the raw volume of parcellated voxels are listed in cubic millimeters (Figure 25). These values are the average of all 20 amygdala subnuclei volumes for each individual nucleus. The relative volumes of amygdala subnuclei as sums of the whole structure's volumetry are depicted in a pie chart.

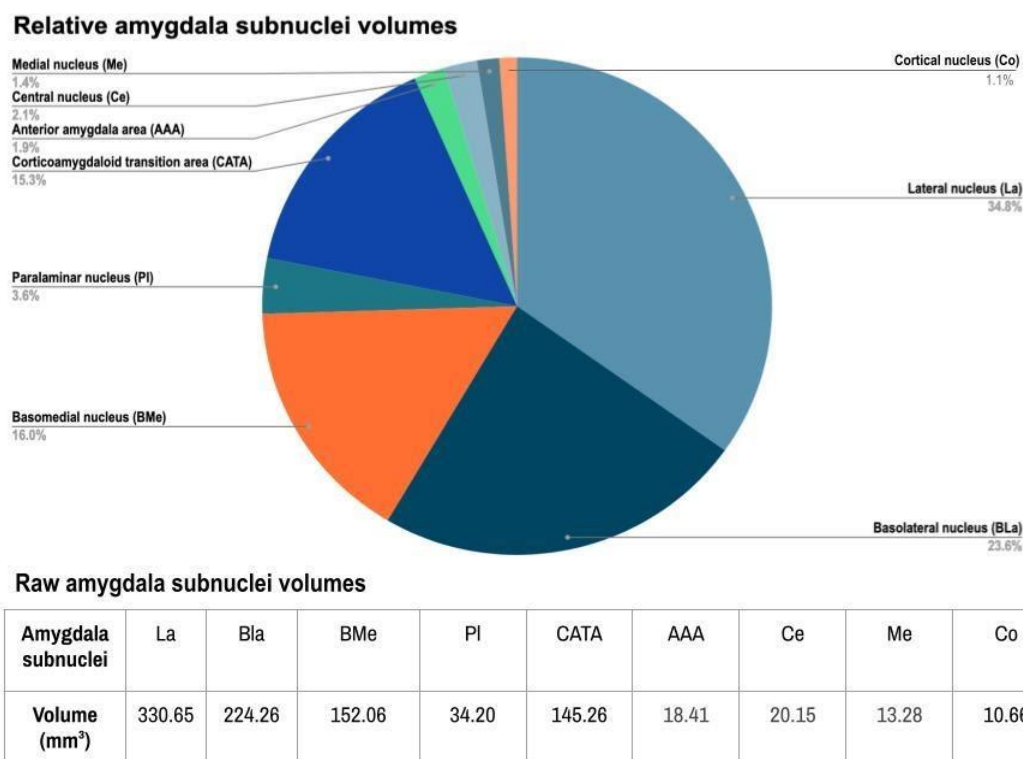


Figure 25. The raw and relative amygdala subnuclei volumes. Abbreviations: Lateral nucleus (La); Basolateral nucleus (BLa); Basomedial nucleus (BMe); Paralaminar nucleus (PL); Corticoamygdaloid transition area (CATA); Anterior amygdala area (AAA); Central nucleus (Ce); Medial nucleus (Me); Cortical nucleus (Co).

The largest amygdala subnuclei together composing 75% of the relative total amygdala volume are the three subnuclei that make up the BLA complex nuclei followed by the PL and CATA nuclei. The smallest amygdala subnuclei in descending order are the central, AAA, medial and cortical nuclei.

3.3 Manual segmentation reliabilities of amygdala subnuclei volumes

The manual segmentation protocol for the amygdala subnuclei can be validated for its repeatability and reliability through the determination of the dice similarity coefficients (Table 3) and intraclass correlation coefficients (Table 4) both by intra-rater SP as well as by inter-raters SP and DC.

| Amygdala subnuclei | La | BLa | BMe | PL | CATA | AAA | Ce | Me | Co |
|--|-----------------|-----------------|-----------------|-----------------|-----------------|-----------------|-----------------|-----------------|-----------------|
| Intra-rater reliability \pm SD | 0.86 \pm 0.02 | 0.82 \pm 0.03 | 0.77 \pm 0.04 | 0.75 \pm 0.09 | 0.79 \pm 0.02 | 0.71 \pm 0.04 | 0.72 \pm 0.05 | 0.68 \pm 0.03 | 0.64 \pm 0.01 |
| Inter-rater reliability \pm SD | 0.83 \pm 0.03 | 0.78 \pm 0.01 | 0.73 \pm 0.04 | 0.72 \pm 0.06 | 0.73 \pm 0.03 | 0.59 \pm 0.06 | 0.57 \pm 0.06 | 0.59 \pm 0.05 | 0.51 \pm 0.03 |

Table 3. The dice kappa intra and inter-rater coefficient reliabilities for the nine manually segmented subnuclei. Abbreviations: Lateral nucleus (La); Basolateral nucleus (BLa); Basomedial nucleus (BMe); Paralaminar nucleus (PL); Corticoamygdaloid transition area (CATA); Anterior amygdala area (AAA); Central nucleus (Ce); Medial nucleus (Me); Cortical nucleus (Co).

| Amygdala subnuclei | La | BLa | BMe | PL | CATA | AAA | Ce | Me | Co |
|--------------------|------|------|------|------|------|------|------|------|------|
| Intra-rater | 0.97 | 0.96 | 0.95 | 0.92 | 0.91 | 0.88 | 0.89 | 0.85 | 0.76 |
| Inter-rater | 0.94 | 0.92 | 0.91 | 0.87 | 0.84 | 0.80 | 0.84 | 0.82 | 0.72 |

Table 4. The intraclass correlation coefficients for intra and inter-rater reliabilities as applied to the nine manually segmented subnuclei. Abbreviations: Lateral nucleus (La); Basolateral nucleus (BLa); Basomedial nucleus (BMe); Paralaminar nucleus (PL); Corticoamygdaloid transition area (CATA); Anterior amygdala area (AAA); Central nucleus (Ce); Medial nucleus (Me); Cortical nucleus (Co).

Both the intra- and inter-rater dice similarity and intraclass correlation coefficients suggest that the manual segmentation protocol outlined in this work is highly reliable and repeatable. ICC values over 0.90 especially suggest a highly repeatable protocol as seen more so in the intra-rater but also inter-rater ICC. The largest BLA subnuclei are the most evident and easiest to segment and as such this is reflected in the high intra and inter-rater

ICC and dice kappa coefficient scores. In contrast, the smallest, most difficult to segment cortical subnucleus sees the lowest scores in all categories.

The Dice kappa coefficients were also determined for the comparison between the Saygin automated amygdala subnuclei atlas and the manual segmentation protocol developed in the current study for two ultra-high resolution MRI and histology datasets (Table 5).

| | 7T Edlow MRI | BigBrain Histology |
|--|-------------------------------|-------------------------------|
| Amygdala subnuclei | Dice kappa coefficient | Dice kappa coefficient |
| Lateral nucleus (La) | 0.83 | 0.85 |
| Basolateral nucleus (BLa) | 0.80 | 0.82 |
| Basomedial nucleus (BMe) | 0.84 | 0.79 |
| Paralaminar nucleus (PL) | 0.74 | 0.75 |
| Corticoamygdaloid transition area (CATA) | 0.78 | 0.82 |
| Anterior amygdala area (AAA) | 0.63 | 0.72 |
| Central nucleus (Ce) | 0.69 | 0.68 |
| Medial nucleus (Me) | 0.65 | 0.64 |
| Cortical nucleus (Co) | 0.50 | 0.53 |

Table 5. The dice kappa coefficients for nine segmented amygdala subnuclei compared manually and automatically for two datasets.

Chapter 4

4 Discussion

The amygdala is a challenging brain structure to discern amongst its anatomically heterogeneous yet seemingly homogenous grey matter islet subnuclei. At lower strength magnetic field MRI scanners, amygdala subnuclei cannot be distinguished.

Neuroimaging studies at higher magnetic field strength scanners bring promise in the ability to visualize subcortical structures. In taking advantage of an ultra-high magnetic field strength 9.4T MRI scanner, we were able to depict and parcellate nine amygdala subnuclei and determined that the segmentation protocol yielded high intra- and inter-rater dice kappa and intraclass correlation coefficient scores suggesting highly reproducible protocol results.

4.1 Ultra-high field MRI amygdala segmentation

Ultra-high field MRI studies investigating amygdala functions *in-vivo* lead to volumetric results just as they do in *ex vivo* examinations. With *in-vivo* participant scanning, whole amygdala structure volumes are outputted for quantitative measures. In an ultra-high field 7T MRI study, an automated amygdala template generated for an Alzheimer's disease cohort included four subgroups: basolateral, basomedial, lateral, and centromedial⁶⁴. Significant atrophy as determined by reduced voxel volumes was found in the basolateral and basomedial subregions of the amygdala. The individual subnuclei of the amygdala could not clearly be delineated from each other in another 7T MRI paper acquiring *in-vivo* T1-weighted images⁶⁵. In a comparison study of epilepsy patients and healthy control cases conducted at 7T MRI, the amygdala was automatically labelled in its entirety by a convolutional neural network resulting in high dice kappa coefficient segmentation scores⁶⁶. Ultra-high field magnetic field strength scanners are classified at those 7T and above. While 7T MRI acquisition methods are employed in *in-vivo* research studies, not all individual amygdala subnuclei can be clearly delineated even at ultra-high field strength.

Ex vivo specimens are the most precious resource when investigating brain structure in MRI neuroimaging data acquisitions. With post-mortem MRI data collection, several

limitations present with *in-vivo* neuroimaging such as scanning time length are not applicable. With combined long scan times of non-moving objects, high spatial resolution MRI images may result and there is greater promise in the ability to visualize similarly appearing yet distinct amygdala subnuclei. The image contrast collected at ultra-high resolution *ex vivo* MRI imaging has resulted in an abundance of hippocampus manual segmentation and automated atlas developments^{67, 68, 69}. In many of these cases, the amygdala region and its subnuclei are simply afterthoughts not included in protocols or quantitative measure outcomes.

Because the visualization of amygdala subnuclei is difficult, it is an appreciably understudied structure compared to the hippocampus. Saygin and colleagues developed an *ex vivo* atlas of nine amygdala subnuclei at 7T MRI that became publicly available to be propagated onto any naïve MRI data⁵⁵. The individual subnuclei segmented in the current study at 9.4T were the same as those managed in the Saygin paper. A preliminary study of *ex vivo* rhesus monkeys at 9.4T MRI revealed a decent distinction between the BLA nuclei but not among any of the rest⁷⁰. While the elucidation of white matter tracts rather than manual segmentation of nuclei was the focus of one paper, their comparison between post-mortem MRI and histology showed that almost all amygdala subnuclei could be distinguished clearly in their presented figures with MRI images obtained from a 11.7T Bruker MRI scanner⁷¹. The resolution of the amygdala subnuclei absolutely requires *ex vivo* ultra-high field data collection. We are the first to outline a manual segmentation protocol for the delineation of the nine amygdala subnuclei at 9.4T MRI.

4.2 Amygdala subnuclei segmentation protocols

Despite the limited attempts at imaging the amygdala subnuclei at ultra-high field MRI either *in vivo* or *ex vivo* to obtain volumetric and morphometric data, there still remains a lack of cohesive agreement on the mechanisms of amygdala subnuclei segmentation. Many studies present a very brief protocol of the ways in which to parcellate the amygdala subnuclei. In these segmentation protocols, the rules for delineating each nucleus can be considered subjective as it is usually in relation to other neighbouring subnuclei, which are all challenging to discern. The segmentation steps are sometimes

simply descriptive rather than segmentation instructions. In the Saygin paper, one of the determinants of the parcellation of the cortical nucleus was quite arbitrary as it stated this nucleus is present in the fewest number of MRI slices; yet not which precise slices nor where. Since it is already hard to tell apart the subnuclei, these written outlines often do not help the clarity or specificity of a protocol.

While the manual segmentation protocol of amygdala subnuclei in the present work is outlined by a short paragraph description for each individual nucleus, there are accompanying figures in the coronal plane moving through the amygdala slices displaying the visual steps in the manual segmentation for an individual subnucleus. Parcellation decisions are made that aid in the segmentation process overall. This study determined one order in which the amygdala subnuclei should be segmented. For example, we propose that the paralaminar nucleus should be the first nucleus to be segmented. Beginning at the posterior end of the paralaminar nucleus as its image contrast makes it more discernible. This also allows for the identification of the BLA nuclei that are more dorsal to the paralaminar nucleus to be parcelled next with ease. Many lower field strength manual segmentation protocols rely on indirect instructions based upon prior anatomical atlases resulting in the grouping of amygdala subnuclei by geometric rules rather than their true individual parcellation placements⁷⁶. These outcomes may be valid as evidenced by high dice similarity and ICC intra and inter-rater reliabilities, but they do not capture the full neuroanatomy of the human amygdala. The Saygin automated amygdala subnuclei atlas is now a popular choice among neuroimaging researchers as it saves a lot of time in the otherwise very labor intensive manual segmentation process. We decided to anatomically label the amygdala with the same nomenclature. The nine amygdala subnuclei that were parcellated in the current study like that in the Saygin paper are: the lateral, basolateral, basomedial, central, medial, cortical, corticoamygdaloid transition area, paralaminar, and anterior amygdala area nuclei. This nomenclature is also utilized in many physical neuroanatomical texts with photos of the amygdala subnuclei on MRI scans and histological slices that the current protocol has referenced^{13, 64}. In the 11.7T MRI amygdala MRI and histology investigation, amygdala subnuclei were simply outlined instead of parcellated; yet, differences in the naming and grouping of these subnuclei make it challenging to

compare with conventional amygdala subnuclei nomenclature ⁷¹. The researchers united the central and medial subnuclei as a single centromedial group. They labelled the corticoamygdaloid transition area the superficial cortex-like amygdala. We propose the amygdala subnuclei labelling follows that set out in the present study's manual segmentation protocol to garner consensus and avoid confusion of amygdalar neuroanatomy.

4.3 Limitations to amygdala subnuclei segmentation

While with ultra-high field MRI and histology techniques we are able to well characterize the amygdala subnuclei, it is still a challenging task due to the underlying microanatomy of the structure. All amygdala subnuclei are grey matter substructures. Only the central, medial, and anterior amygdala area stand alone and apart from the rest of the nuclei as they are surrounded by white matter. The other subnuclei are huddled together and discriminating amongst them is hard because there are no clear white matter boundaries to separate them. This is especially true looking ventrally in the coronal plane. These difficulties apply not only to lower magnetic field strength studies where solely the amygdala as a whole can be visualized but also in scans obtained at the highest magnetic field strengths, 7T, 9.4T and 11.7T.

Diffusion MRI is a method of imaging the white matter fibers within the brain by tracking the movement of water molecules within the fibre tracts. Although the amygdala is not known for its distinctive white matter tract fibre anatomy that separates its subregions, several studies have tried this technique to determine if subnuclei characterization is made easier. In a 3T diffusion study, the *in-vivo* amygdala was divided into three regions as a result of a spatial clustering algorithm ⁷². The algorithm used the principal diffusion direction in each amygdala voxel creating a reliable separation into medial and lateral divisions consistent with the fiber architecture visible in myelin-stained *ex vivo* amygdala slices. Post-mortem data collected at 11.7T MRI saw diffusion MRI carve white matter tracts between some amygdala subnuclei ⁷¹. It revealed intra-amygdalar laminar white matter fibers, especially between the BLA subnuclei, allowing for a clearer 3D reconstruction of the structure. Even so, intra-amygdalar laminar partitions did not exist surrounding each and every nucleus. The main objective of the

study was to elucidate the extended amygdala substructures like the white matter stria terminalis fibre rather than discriminating the subnuclei. While employment of ultra-high field scanners leads to challenges in determining amygdala subnuclei differences, diffusion MRI acquisition techniques are still not quite helpful in delineating subnuclei boundaries because of the underlying cellular composition of the structure.

Post-mortem ultra-high field MRI image acquisition is only the second best method of characterizing the amygdala subnuclei. Collecting histological staining through amygdala slices aids in determining a reference ground standard of subnuclei locations. One limitation of the current study is the lack of histology acquisition for at least one of the *ex vivo* specimens. Instead, we relied on neuroanatomical textbooks which showed histology images as examples and from which the manual segmentation protocol for the amygdala was derived. Had we had access to histology amygdala slices to register and compare the MRI scans with, we would have had a more accurate portrayal of the subnuclei distinctions on which to base the protocol. Another limitation is that the number of post-mortem specimens is small with ten donors, and the average age at the time of death was 71.7. While none of the donors passed away from any neurological disease, it is possible they exhibited other brain anatomy pathologies or their beginnings. Brain atrophy localized to the amygdala has been found in patients with early Alzheimer's disease ⁷⁹. Several studies have however noted that age does not have an impact on the volume of the amygdala ⁸⁰. Amygdala volumes seem to increase in childhood and stabilize once reaching early adulthood ⁸¹.

Amunts and colleagues were the first to map the human amygdala in terms of its cytoarchitecture ⁷⁷. They first stained ten post-mortem specimens using the Merker silver staining method painting cell bodies dark compared to the lighter colour presented white matter to visualize the amygdala subnuclei boundaries. Prior to staining, the amygdala portions were scanned with MRI at 1.5T. Probabilistic and stereotaxic anatomical maps were created. Although the amygdala subnuclei could be distinguished on the histological slices, on their mappings onto the MRI images, the subnuclei were gathered into groupings. The anatomists concluded higher spatial resolution and contrast would be

necessary in the MRI acquisition process to determine a more comprehensive cytoarchitecture mapping of amygdala subnuclei.

Looking for the amygdala subnuclei at ultra-high field 9.4T MRI or the high-resolution whole brain scan acquisition at 7T MRI by Edlow is not sufficient to observe the microanatomy of each subnucleus that would otherwise determine cellular distinctions amongst them. When observing the amygdala subnuclei obtained from the high-resolution histological database BigBrain, it is still challenging to depict the boundaries when zooming into the more molecular level. At the histological level, the intercalated cell nuclei of the human amygdala continue to remain unseen. Outside of the extended amygdala, the IC nuclei would represent the tenth amygdala subregion in addition to the nine outlined. The IC nuclei may be more of a marker pertinent to animal neuroanatomy appearing as a darker teardrop shape between the BLA and central and medial nuclei ⁷³. All other BigBrain amygdala subnuclei were parcellated with ease. We suggest that the nine human amygdala subnuclei segmented in the present study should be kept consistent and applied across any future parcellations in terms of nomenclature and instruction.

4.4 Amygdala subnuclei manual segmentation reliabilities

The main quantitative outcomes of the manual segmentation protocol for the *ex vivo* amygdala subnuclei are the intra and inter-rater dice kappa and intraclass correlation coefficients. The intra-rater reliabilities of rater SP were higher than the inter-rater reliability scores for both measures. This is to be expected as the manual segmentation protocol was developed by SP. The intra-rater reliabilities for the intraclass correlation and dice kappa coefficients were highest for the BLA, CATA, and PL nuclei while the cortical nucleus consistently saw the lowest reliability scores. The same substructure patterns followed for the inter-rater reliability scores between SP and DC. The largest nuclei by volume are also the subnuclei with the higher coefficient values because they are more evident subregions to discern. ICC values over 0.90 represent the highest reliability. The BLA nuclei are the most highly valid manually segmented nuclei. Contraversely, the smallest and hardest to segment cortical subnucleus consistently exhibit the lowest intra and inter-rater dice kappa and intraclass correlation

coefficient values. The cortical nucleus example presented in the current study exhibited one of the most evident boundaries for delineating this particular subregion but in most other scanned amygdala portions, it was impossible to make out (Figure 19). The manual segmentation protocol reliability is largely dependent on the ease with which the amygdala subnuclei can be determined.

In a separate but related comparison, the Freesurfer 7.1 amygdala subnuclei automated atlas created by Saygin and colleagues was applied onto the high-resolution Edlow MRI and BigBrain histology data manually segmented by SP. The protocols in the Saygin paper were very similar to those in the current study presentation in terms of amygdala subnuclei nomenclature and localization. The dice kappa coefficient values were moderate to low in both intra-rater cases when comparing the automated Saygin amygdala subnuclei atlas to the manual tracing protocol set forth in the current study. The dice kappa coefficients are moderately high at values in the range of 0.80 to 0.90 for the BLA nuclei but rather low for the others in both the ultra high-resolution histology and MRI datasets. Since great care was taken to segment the amygdala subnuclei manually as precisely as possible in the two ultra high-resolution images, these values suggest the automated atlas volumetric outputs should be interpreted with caution when applied to other datasets. The compared manual and automated segmentations cannot be relied upon confidently in the case of both the 7T Edlow and BigBrain histology amygdala images. One study employed Sayin's FreeSurfer amygdala subnuclei atlas in their investigation of major depressive disorder patients and found that many of the subregions of the amygdala were volumetrically reduced in correlation with worsening depressive symptoms⁵⁴. In their mapping of the atlas onto the MRI scans, the association of the nuclei onto their correct anatomical locations is slightly off, similar to the automated atlas in Figure 23. While they found no differences in symptom severity correlations among the different subnuclei, the anatomical locations weren't quite lined up correctly and as such these results should be met with some consideration for protocol accuracy and therefore volumetric results.

4.5 Amygdala subnuclei segmentation enhancements

Although limited, great strides have been made in the close-up investigation of the delineation of the human amygdala subnuclei. Ultra-high field MRI studies have pushed the limits. With *ex vivo* data collection at 7T MRI and above, the nine amygdala subnuclei can be parcellated individually. An automatic amygdala subnuclei was created based upon specimens imaged at 7T, and a side-by-side MRI and histology co-registration study outlined the same nuclei at 11.7T yet did not perform segmentations for volumetric outputs. We were the first to attempt to visualize and trace the amygdala subnuclei using a 9.4T MRI scanner.

It would be beneficial to adhere to a singular clear-cut amygdala subnuclei anatomical instructional outline for all future protocols. This would ensure unity in both the naming and tracing guidance for the structure and its subregions. The Hippocampal Subfields Group (<http://hippocampalsubfields.com>) is composed of principal investigators from several research laboratories who discuss and consolidate manual segmentation protocols for the hippocampus structure which neighbours the amygdala. Researchers involved and interested in the amygdala subnuclei's macroscopic level anatomy and microanatomy should convene to consider whether such a protocol like the one proposed in the current study seems reasonable and accurate. Neuroanatomy texts are insufficient references in determining boundaries on MRI scans. A consensus must be made moving forward by researchers and neuroanatomists. One small potential improvement to the proposed protocol is the segmentation of the whole amygdala structure in advance of the individual amygdala subnuclei parcellations. It is often easier to outline and trace the amygdala structure in its entirety than it is to discriminate its subregions, and a rater could make better decisions on which subnuclei are bound within the confines of the predefined whole amygdala volume.

Obtaining top quality high-resolution histological and MRI images of the same specimens must be a requirement to validate registration and manual segmentation protocols. We compared the most ultra high-resolution MRI and histology datasets publicly available when applying the automated Saygin atlas. Yet to procure MRI and histology data from the same specimen would yield the best opportunity for amygdala

subnuclei tracing protocols and likely even more precise volumetric measurements. Manual registration preceding manual segmentation of the human amygdala scanned using MRI and co-registered to its histology is a must. This would ensure that neuroanatomical characteristics unable to be picked up on an MRI image could be inferred by referencing the identical specimen's histological slices as opposed to those from an example text of a completely different specimen. The BigBrain histological data is unique because the *ex vivo* specimen was very thinly sliced with a microtome acquiring slices capturing the entire amygdala region with great detail. With a clinical specimen of the amygdala we obtained to test scan with our 9.4T MRI acquisition parameters, there were only three slices that were able to be histologically processed by a pathologist (Figure 26). In this case, the equipment and time necessary to procure histology slices through as many of the slices which appear in its corresponding ultra high-resolution amygdala MRI scan could not be accomplished. This removes the possibility of determining precise volumetric measurements in reference to the histological scans because only three of many MRI acquired slices have their reference histology slice available for viewing. HistoloZee is an interactive tool that was used to align the amygdala MRI to its histological slice counterpart (www.nitrc.org/projects/historecon). The clinical histology processing used hematoxylin and eosin staining where purple colouring represents the brain's white matter and pink the grey matter.

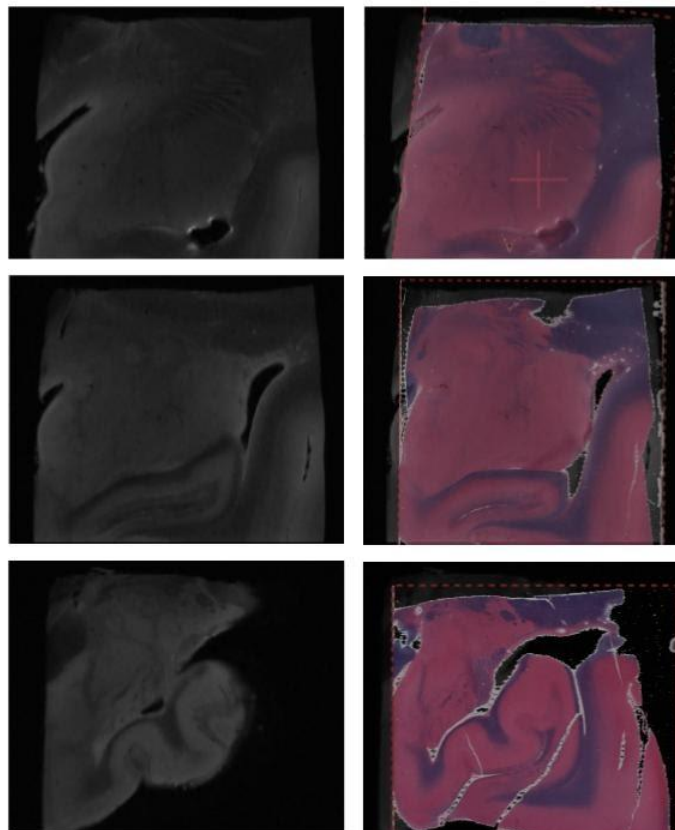


Figure 26. A clinical human amygdala specimen with three processed histological slices on the right hand side co-registered with the 9.4T MRI scans presented on the left.

4.6 Future applications

Although the main objective of the current study was to visualize the amygdala subnuclei neuroanatomy at ultra-high field strength MRI, many applications may follow. For one, an automated amygdala subnuclei atlas in slight improvement from the Saygin automated amygdala atlas can be developed in-house. The Saygin paper also acquired ten post-mortem human amygdala specimens at ultra-high field MRI. However, while their automated amygdala subnuclei is now publicly available and beginning to be used by many other research laboratories, it is important to note its output may not be anatomically correct in all instances. In the present study prior to the segmentation of the amygdala projections acquired at 9.4T MRI, we registered them onto the whole brain *ex vivo* specimens from which they were derived and themselves scanned at 7T. The

registration between the 9.4T amygdala samples onto their corresponding locations on the whole brain 7T scans using four anatomical landmark fiducials, all produced low target registration errors overall. Since the whole brain specimens were preprocessed and registered to a common brain template called MNI, the amygdala scans were therefore also registered relatively well into the same template. This is one big advantage over the Saygin automated amygdala atlas as this registration onto a template will allow for greater accuracy when projected onto any other MRI dataset once it too is automatically registered to the same MNI template. In this way, we will have more confidence in not only the anatomical placement of amygdala subnuclei but also any volumetric metrics and statistical analyses.

The proposed amygdala subnuclei protocol will also become beneficial in clinical neuropathological work like that introduced in Figure 26. The amygdala plays an important role in the development and progression of many neurological disorders. Amygdala dysfunction may be a marker for sudden unexpected death in epilepsy (SUDEP)⁸². The pathophysiology and pathology of the amygdala is implicated in epilepsy and epileptogenesis⁸³. Anecdotal evidence in patients about to experience the onset of a seizure have self-reported the smell of burning toast. It may be possible that the medial nucleus of the amygdala, known to have olfactory function, is a subnuclei unique to the occurrence or onset of a seizure. With an automated amygdala subnuclei atlas, this function could be investigated further structurally or functionally.

The amygdala brain structure is best recognized for its known involvement in the fight, flight, or freeze fear response. We have acquired much knowledge in the macroscopic detail of the structure and its subnuclei. With the development of a generated automated anatomical mapping that we could easily overlay onto a participant's MRI scan *in-vivo* while they perform a daunting task with a joystick or lie still and watch a horror movie clip, and we will be able to describe which amygdala subnuclei in particular are more susceptible to scary moments in the performance of fMRI studies.

4.7 Conclusion

We have developed a protocol for segmenting the human amygdala subnuclei that was only made possible by the employment of an ultra-high field magnetic resonance 9.4T scanner. This yielded high-resolution depictions of the difficult to distinguish grey matter subnuclei of the amygdala that allowed for their visualization and discernment. The manual tracing protocol we developed included helpful suggestions that resulted in high intra and inter-rater reliabilities and confidence in those same reliabilities. We exhausted the field of ultra high-resolution data by investigating the amygdala's structure within other high quality datasets available. Our proposed suggestions in bringing unity and coming to a consensus about the manual segmentation of amygdala subnuclei are warranted at a time of limited expertise in the neuroanatomy of this structure. Future applications of a developed automated atlas derived from this work will be more reliable when applied to clinical or psychological studies of amygdala subnuclei function because of our great strides in structural precision.

References

1. Furmark, T., Fischer, H., Wik, G., Larsson, M. & Fredrikson, M. The amygdala and individual differences in human fear conditioning. *NeuroReport* **8**, 3957–3960 (1997)
2. Thesen, T., Vibell, J. F., Calvert, G. A. & Österbauer, R. A. Neuroimaging of multisensory processing in vision, audition, touch, and olfaction. *Cogn Process* **5**, 84–93 (2004).
3. Buser, P. & Bancaud, J. Unilateral connections between amygdala and hippocampus in man. A study of epileptic patients with depth electrodes. *Electroencephalography and Clinical Neurophysiology* **55**, 1–12 (1983).
4. Burdach, K. F. *Vom Baue und Leben des Gehirns*. (Dyk, 1826).
5. Meynert, T. Der Bau der Gross-Hirnrinde und seine örtlichen Verschiedenheiten, nebst einem pathologisch-anatomischen Corollarium: separat-Abdruck aus der " Vierteljahrsschrift für Psychiatrie etc.". Heuser; 1872.
6. Johnston, J. B. Further contributions to the study of the evolution of the forebrain. V. Survey of forebrain morphology. *Journal of Comparative Neurology* **36**, 143–192 (1923).
7. Pabba, M. Evolutionary development of the amygdaloid complex. *Front Neuroanat* **7**, 27 (2013).
8. Remedios, R. *et al.* A stream of cells migrating from the caudal telencephalon reveals a link between the amygdala and neocortex. *Nat Neurosci* **10**, 1141–1150 (2007).
9. Huilgol, D. *et al.* Dual origins of the mammalian accessory olfactory bulb revealed by an evolutionarily conserved migratory stream. *Nat Neurosci* **16**, 157–165 (2013).
10. Hall, I. C., Ballagh, I. H. & Kelley, D. B. The Xenopus Amygdala Mediates Socially Appropriate Vocal Communication Signals. *J Neurosci* **33**, 14534–14548 (2013).
11. Moreno, N. & González, A. Localization and connectivity of the lateral amygdala in anuran amphibians. *J Comp Neurol* **479**, 130–148 (2004).
12. Bruce, L. L. & Neary, T. J. The Limbic System of Tetrapods: A Comparative Analysis of Cortical and Amygdalar Populations. *Brain Behav Evol* **46**, 224–234 (1995).
13. Di Marino, V., Etienne, Y., & Niddam, M. The amygdaloid nuclear complex. Cham: Springer. 2016.
14. Rubenstein, J. L. R., Martinez, S., Shimamura, K., & Puelles, L. The Embryonic Vertebrate Forebrain: the Prosomeric Model. *Science* **266**, 578-580 (1994).
15. Crosby, E. C., Humphrey, T., & Lauer, E. W. Correlative anatomy of the nervous system. The Macmillan company, New-York (1962).
16. Adolphs, R., Tranel, D., Damasio, H. & Damasio, A. Impaired recognition of emotion in facial expressions following bilateral damage to the human amygdala. *Nature* **372**, 669–672 (1994).
17. Tranel, D., Gullickson, G., Koch, M. & Adolphs, R. Altered experience of emotion following bilateral amygdala damage. *Cogn Neuropsychiatry* **11**, 219–232 (2006).

18. Laberge, F., Mühlenbrock-Lenter, S., Grunwald, W. & Roth, G. Evolution of the Amygdala: New Insights from Studies in Amphibians. *BBE* **67**, 177–187 (2006).
19. Dielenberg, R. A., Hunt, G. E. & McGregor, I. S. ‘When a rat smells a cat’: the distribution of Fos immunoreactivity in rat brain following exposure to a predatory odor. *Neuroscience* **104**, 1085–1097 (2001).
20. Brockhaus, H. Zur normalen und pathologischen Anatomie der Mandelkerngebiete. *J Psycholo Neurol* **49**, 1-136 (1938).
21. De Olmos, J. S. Amygdala. In: Praxinos, G., Mai, J. K. The human nervous system. *Elsevier*, Amsterdam, 739-868 (2004).
22. AbuHasan, Q., Reddy, V. & Siddiqui, W. Neuroanatomy, Amygdala. in *StatPearls* (StatPearls Publishing, 2021).
23. Alheid, G. F. & Heimer, L. New perspectives in basal forebrain organization of special relevance for neuropsychiatric disorders: the striatopallidal, amygdaloid, and corticopetal components of substantia innominata. *Neuroscience* **27**, 1–39 (1988).
24. deCampo, D. & Fudge, J. Where and what is the paralaminar nucleus? A review on a unique and frequently overlooked area of the primate amygdala. *Neurosci Biobehav Rev* **36**, 520–535 (2012).
25. Lebow, M. A. & Chen, A. Overshadowed by the amygdala: the bed nucleus of the stria terminalis emerges as key to psychiatric disorders. *Mol Psychiatry* **21**, 450–463 (2016).
26. Fudge, J. L. & Emiliano, A. B. The Extended Amygdala and the Dopamine System: Another Piece of the Dopamine Puzzle. *J Neuropsychiatry Clin Neurosci* **15**, 306–316 (2003).
27. Alheid, G. F. Extended Amygdala and Basal Forebrain. *Annals of the New York Academy of Sciences* **985**, 185–205 (2003).
28. Fudge, J. L. & Tucker, T. Amygdala projections to central amygdaloid nucleus subdivisions and transition zones in the primate. *Neuroscience* **159**, 819–841 (2009).
29. Kalin, N. H. The Role of the Central Nucleus of the Amygdala in Mediating Fear and Anxiety in the Primate. *Journal of Neuroscience* **24**, 5506–5515 (2004).
30. Neugebauer, V. 15. Amygdala pain mechanisms. *Handb Exp Pharmacol* **227**, 261–284 (2015).
31. LeDoux J. The amygdala. *Curr Biol* **17**, R868-R874 (2007).
32. Campeau, S. & Davis, M. Involvement of subcortical and cortical afferents to the lateral nucleus of the amygdala in fear conditioning measured with fear-potentiated startle in rats trained concurrently with auditory and visual conditioned stimuli. *J. Neurosci.* **15**, 2312–2327 (1995).
33. Stefanacci, L. *et al.* Projections from the lateral nucleus to the basal nucleus of the amygdala: A light and electron microscopic PHA-L study in the rat. *Journal of Comparative Neurology* **323**, 586–601 (1992).
34. Marsh, R. A., Fuzessery, Z. M., Grose, C. D. & Wenstrup, J. J. Projection to the Inferior Colliculus from the Basal Nucleus of the Amygdala. *J. Neurosci.* **22**, 10449–10460 (2002).

35. Carlson, N. R. *Physiology of behavior*. (Boston : Pearson, 2013).
36. Quirk, G. J. & Mueller, D. Neural Mechanisms of Extinction Learning and Retrieval. *Neuropsychopharmacology* **33**, 56–72 (2008).
37. Busti, D. *et al.* Different Fear States Engage Distinct Networks within the Intercalated Cell Clusters of the Amygdala. *J Neurosci* **31**, 5131–5144 (2011).
38. Smith, C. A. & Kirby, L. D. Toward delivering on the promise of appraisal theory in *Appraisal processes in emotion: Theory, methods, research* 121–138 (Oxford University Press, 2001).
39. Pikkarainen, M., Rönkkö, S., Savander, V., Insausti, R. & Pitkänen, A. Projections from the lateral, basal, and accessory basal nuclei of the amygdala to the hippocampal formation in rat. *Journal of Comparative Neurology* **403**, 229–260 (1999).
40. Fudge, J. L. & Tucker, T. Amygdala projections to central amygdaloid nucleus subdivisions and transition zones in the primate. *Neuroscience* **159**, 819–841 (2009).
41. Rauch, S.L. *et al.* Exaggerated amygdala response to masked facial stimuli in posttraumatic stress disorder: a functional MRI study. *Biological psychiatry* **47**(9), pp.769-776 (2000).
42. Usher, J., Leucht, S., Falkai, P. & Scherk, H. Correlation between amygdala volume and age in bipolar disorder — A systematic review and meta-analysis of structural MRI studies. *Psychiatry Research: Neuroimaging* **182**, 1–8 (2010).
43. Brabec, J. *et al.* Volume of the amygdala is reduced in patients with narcolepsy – a structural MRI study. **5** (2011).
44. Hamilton, J. P., Siemer, M. & Gotlib, I. H. Amygdala volume in major depressive disorder: a meta-analysis of magnetic resonance imaging studies. *Mol Psychiatry* **13**, 993–1000 (2008).
45. Kovacevic, M. *et al.* Amygdala Volumes in Autism Spectrum Disorders: Meta-Analysis of Magnetic Resonance Imaging Studies. *Rev J Autism Dev Disord* (2021).
46. Hashempour, N. *et al.* A Novel Approach for Manual Segmentation of the Amygdala and Hippocampus in Neonate MRI. *Frontiers in Neuroscience* **13**, 1025 (2019).
47. Yushkevich, P. A. *et al.* Quantitative Comparison of 21 Protocols for Labeling Hippocampal Subfields and Parahippocampal Subregions in In Vivo MRI: Towards a Harmonized Segmentation Protocol. *NeuroImage* **111**, 526–541 (2015).
48. Symms, M., Jäger, H. R., Schmierer, K. & Yousry, T. A. A review of structural magnetic resonance neuroimaging. *Journal of Neurology, Neurosurgery & Psychiatry* **75**, 1235–1244 (2004).
49. Pruessner, J. C. *et al.* Volumetry of Hippocampus and Amygdala with High-resolution MRI and Three-dimensional Analysis Software: Minimizing the Discrepancies between Laboratories. *Cerebral Cortex* **10**, 433–442 (2000).
50. Aghamohammadi-Sereshki, A., Huang, Y., Olsen, F. & Malykhin, N. V. In vivo quantification of amygdala subnuclei using 4.7 T fast spin echo imaging. *NeuroImage* **170**, 151–163 (2018).

51. Mai, J., Majtanik, M., & Paxinos, G. Atlas of the human brain. Elsevier, Academic Press (2015).
52. Despotović, I., Goossens, B. and Philips, W. MRI segmentation of the human brain: challenges, methods, and applications. *Computational and mathematical methods in medicine* (2015).
53. Solano-Castiella, E. *et al.* Parcellation of human amygdala in vivo using ultra high field structural MRI. *NeuroImage* **58**, 741–748 (2011).
54. The Human Hippocampus: Functional Anatomy, Vascularization and Serial Sections with MRI, 3rd edition. *AJNR Am J Neuroradiol* **26**, 2702 (2005).
55. Saygin, Z. M. *et al.* High-resolution magnetic resonance imaging reveals nuclei of the human amygdala: manual segmentation to automatic atlas. *Neuroimage* **155**, 370–382 (2017).
56. Brown, S. S. G. *et al.* Structural MRI at 7T reveals amygdala nuclei and hippocampal subfield volumetric association with Major Depressive Disorder symptom severity. *Sci Rep* **9**, 10166 (2019).
57. Fedorov, A. *et al.* 3D Slicer as an Image Computing Platform for the Quantitative Imaging Network. *Magn Reson Imaging* **30**, 1323–1341 (2012).
58. Yushkevich, P. A., Gao, Y. & Gerig, G. ITK-SNAP: an interactive tool for semi-automatic segmentation of multi-modality biomedical images. *Conf Proc IEEE Eng Med Biol Soc* **2016**, 3342–3345 (2016).
59. Fitzpatrick, J. M. & West, J. B. The distribution of target registration error in rigid-body point-based registration. *IEEE Trans Med Imaging* **20**, 917–927 (2001).
60. Taha, A. A. & Hanbury, A. Metrics for evaluating 3D medical image segmentation: analysis, selection, and tool. *BMC Med Imaging* **15**, 29 (2015).
61. Dice, Lee R. Measures of the Amount of Ecologic Association Between Species. *Ecology* **26** (3), 297–302 (1945).
62. Gerig, G., Jomier, M. & Chakos, M. Valmet: A New Validation Tool for Assessing and Improving 3D Object Segmentation. in *Medical Image Computing and Computer-Assisted Intervention – MICCAI 2001* (eds. Niessen, W. J. & Viergever, M. A.) 516–523 (Springer Berlin Heidelberg, 2001).
63. Miller, M. I. *et al.* Amygdalar atrophy in symptomatic Alzheimer’s disease based on diffeomorphometry: the BIOCARD cohort. *Neurobiology of Aging* **36**, S3–S10 (2015).
64. Derix, J. *et al.* Visualization of the amygdalo–hippocampal border and its structural variability by 7T and 3T magnetic resonance imaging. *Hum Brain Mapp* **35**, 4316–4329 (2014).
65. Pardoe, H. R. *et al.* High resolution automated labeling of the hippocampus and amygdala using a 3D convolutional neural network trained on whole brain 700 μm isotropic 7T MP2RAGE MRI. *Hum Brain Mapp* **42**, 2089–2098 (2021).
66. Iglesias, J. E. *et al.* A computational atlas of the hippocampal formation using ex vivo, ultra-high resolution MRI: Application to adaptive segmentation of in vivo MRI. *NeuroImage* **115**, 117–137 (2015).
67. Augustinack, J. C. *et al.* MRI parcellation of ex vivo medial temporal lobe. *Neuroimage* **93 Pt 2**, 252–259 (2014).

68. Delgado-González, J. C. *et al.* Quantitative Measurements in the Human Hippocampus and Related Areas: Correspondence between Ex-Vivo MRI and Histological Preparations. *PLOS ONE* **10**, e0130314 (2015).
69. Chen, H.-Z., Yang, H.-Y., Zhong, K. & Li, J.-L. Preliminary study on fine structures of subcortical nuclei in rhesus monkeys by ex vivo 9.4 T MRI. *Zool Res* **41**, 199–202 (2020).
70. Mori, S. *et al.* Elucidation of White Matter Tracts of the Human Amygdala by Detailed Comparison between High-Resolution Postmortem Magnetic Resonance Imaging and Histology. *Frontiers in Neuroanatomy* **11**, 16 (2017).
71. Solano-Castiella, E. *et al.* Diffusion tensor imaging segments the human amygdala in vivo. *NeuroImage* **49**, 2958–2965 (2010).
72. Lee, S., Kim, S.-J., Kwon, O.-B., Lee, J. H. & Kim, J.-H. Inhibitory networks of the amygdala for emotional memory. *Front Neural Circuits* **7**, 129 (2013).
73. Edlow, B. L. *et al.* 7 Tesla MRI of the ex vivo human brain at 100 micron resolution. *Sci Data* **6**, 244 (2019).
74. Amunts, K. *et al.* BigBrain: an ultrahigh-resolution 3D human brain model. *Science* **340**, 1472–1475 (2013).
75. Entis, J. J., Doerga, P., Barrett, L. F. & Dickerson, B. C. A reliable protocol for the manual segmentation of the human amygdala and its subregions using ultra-high resolution MRI. *NeuroImage* **60**, 1226–1235 (2012).
76. Amunts, K. *et al.* Cytoarchitectonic mapping of the human amygdala, hippocampal region and entorhinal cortex: intersubject variability and probability maps. *Anat Embryol (Berl)* **210**, 343–352 (2005).
77. Merker, B. Silver staining of cell bodies by means of physical development. *J Neurosci Methods* **9**, 235–241 (1983).
78. Poulin, S. P., Dautoff, R., Morris, J. C., Barrett, L. F. & Dickerson, B. C. Amygdala atrophy is prominent in early Alzheimer’s disease and relates to symptom severity. *Psychiatry Res* **194**, 7–13 (2011).
79. Saygin, Z. M. *et al.* Structural Connectivity of the Developing Human Amygdala. *PLOS ONE* **10**, e0125170 (2015).
80. Uematsu, A. *et al.* Developmental Trajectories of Amygdala and Hippocampus from Infancy to Early Adulthood in Healthy Individuals. *PLoS One* **7**, e46970 (2012).
81. Patodia, S. *et al.* Adenosine kinase and adenosine receptors A1R and A2AR in temporal lobe epilepsy and hippocampal sclerosis and association with risk factors for SUDEP. *Epilepsia* **61**, 787–797 (2020).
82. Aroniadou-Anderjaska, V., Fritsch, B., Qashu, F. & Braga, M. F. M. Pathology and pathophysiology of the amygdala in epileptogenesis and epilepsy. *Epilepsy Research* **78**, 102–116 (2008).

Curriculum Vitae

Name: Sara Maria Pac

Post-secondary Education and Degrees: University of Western Ontario
London, Ontario, Canada
2015-2019 B.Sc.

The University of Western Ontario
London, Ontario, Canada
2020-2022 M.Sc. Candidate

Honours and Awards: Neuroscience Travel Award
June 2020

Dean's Honour List
2017, 2018, 2019

Reach for the Top Scholarship
2015

Conference presentations: "Early life adversity and hippocampal maturation in children with autism spectrum disorders"
Organization for Human Brain Mapping (OHBM)
June 2020

"Ultra-high field manual segmentation of the *ex-vivo* human amygdala subnuclei"
Imaging Network of Ontario (IMNO)
March 2021

"Ultra-high field manual segmentation of the *ex-vivo* human amygdala subnuclei"
Organization for Human Brain Mapping (OHBM)
June 2021